

---

# Illustrations

Sang Youn Kim and Jeong Yeon Cho

## Contents

1. Normal Findings: Plain Radiograph and IVU .....	12
2. Normal and Associated Findings: US of the Kidney .....	14
3. Normal Findings: CT of the Kidney.....	17
4. Normal Findings: MRI of the Kidney .....	21
5. Variations of Renal Position .....	24
6. Various Appearances of the Renal Pelvis and Calyx .....	26
7. Vascular Indentations on the Urinary Tract .....	27
8. Renal Backflows .....	30
9. Renal Pseudotumors .....	32
10. Fetal Lobulation .....	39
11. Hilar Lip .....	40
12. Junctional Parenchymal Defect .....	41
13. Renal Unidentified Bright Objects on Ultrasonogram .....	43
14. Sinus Lipomatosis and Prominent Perirenal fat .....	45
15. Pseudohydronephrosis .....	47
16. Ureter: Normal Findings and Variations.....	48
17. Urinary Bladder: Normal Findings and Variations.....	49

---

S.Y. Kim (✉)  
Department of Radiology,  
Seoul National University Hospital, Seoul, Korea  
e-mail: iwishluv@freechal.com, wishluv@empal.com

## 1. Normal Findings: Plain Radiograph and IVU

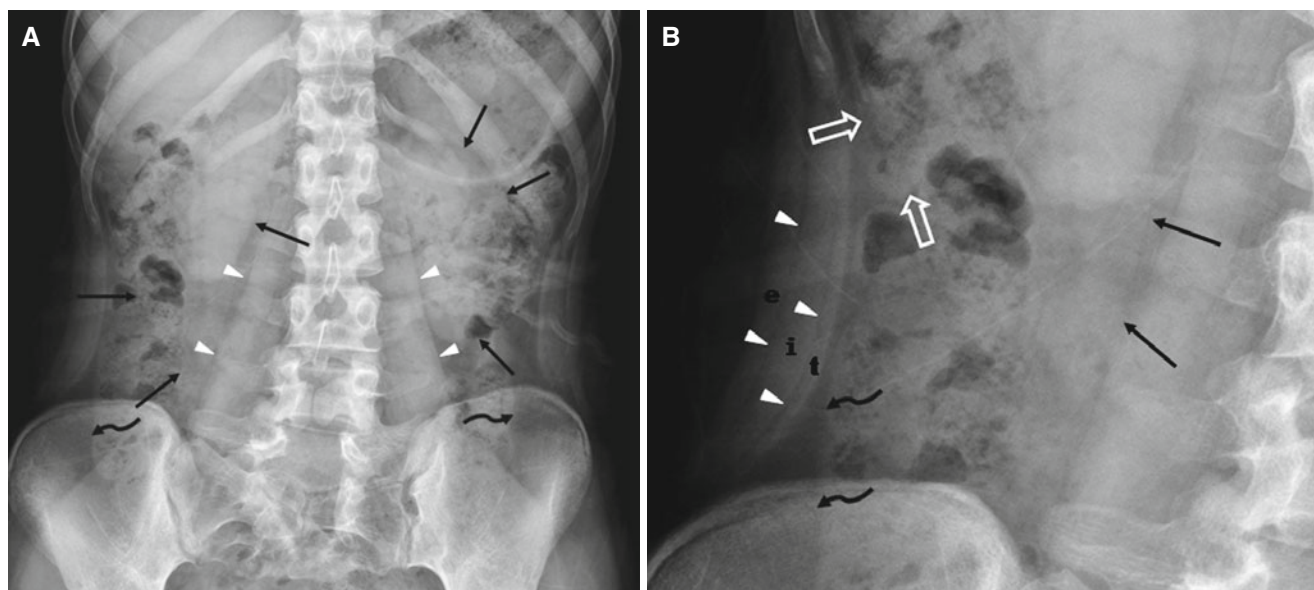


**Fig. 1.1** Normal plain radiograph in a 17-year-old woman. (A) Normal plain radiograph (kidney–ureter–bladder) obtained as a scout image of an IVU well delineates the outlines of the kidneys (*black arrows*) and psoas muscles (*white arrowheads*). Note well-demonstrated properitoneal fat layers or flank stripes (*curved black arrows*). (B) Magnified

image of plain radiograph shows medial margin of the right kidney (*black arrow*), liver edge (*open white arrow*). Also note right properitoneal fat layer (*curved black arrow*) and the fat layers (*white arrowheads*) between the muscles of the abdominal wall. *e* external oblique muscle, *i* internal oblique muscle, *t* transversalis abdominis muscle

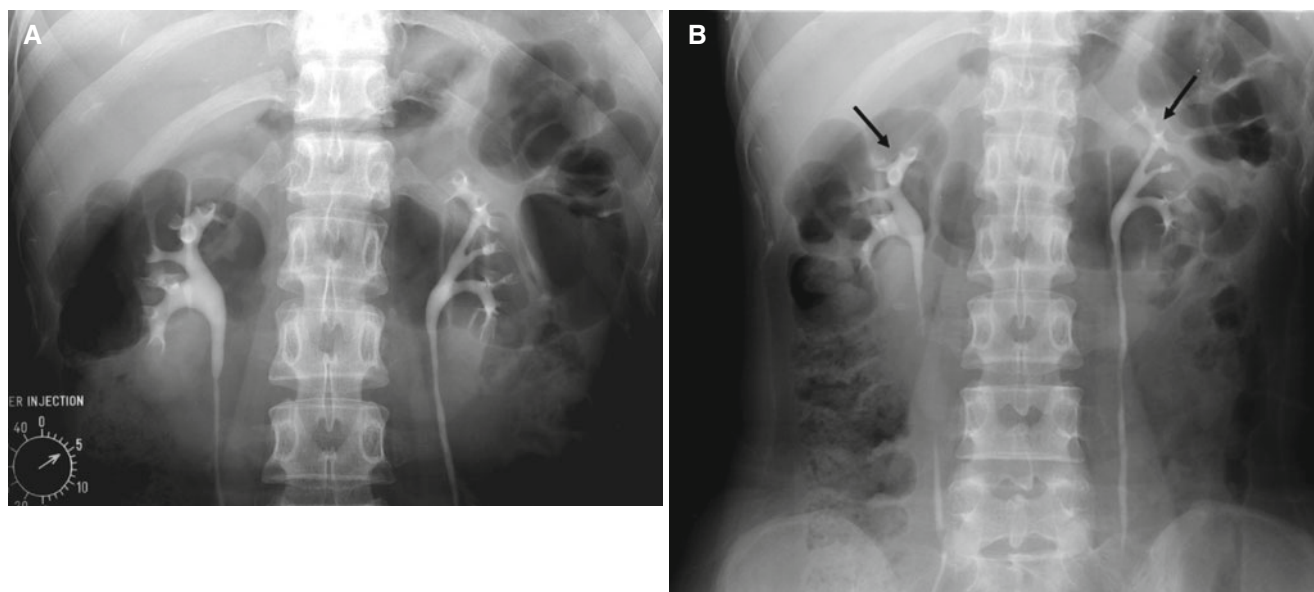


**Fig. 1.2** Normal IVU in a 28-year-old woman. (A) IVU obtained 5 min after injection of contrast material shows various shapes of calyces. (B) 15-min IVU shows well-opacified urinary tracts. Note compound

calyces (*black arrows*) in the upper poles of both kidneys and normal peristaltic contrast flow of both ureters. (C) 30-min IVU shows contrast-filled urinary bladder at the lower aspect of the anatomic pelvis



**Fig. 1.2** (continued)

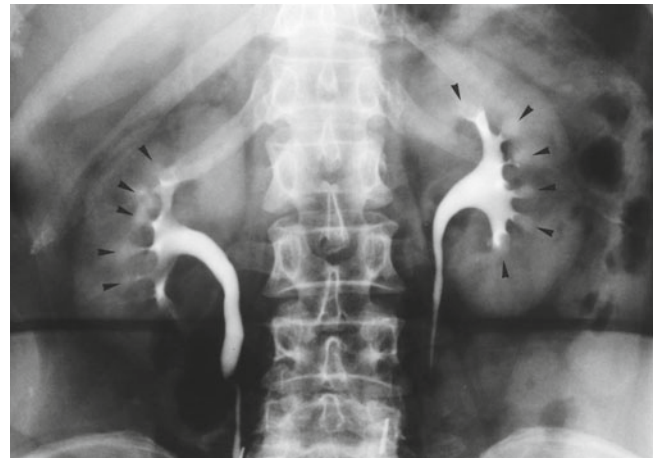


**Fig. 1.3** Normal papillary blush in a 57-year-old woman. IVU taken 15 min after injection of nonionic contrast material shows homogeneous staining of the renal papillae (*black arrowheads*) due to collection of contrast material in normal collecting ducts. Normal papillary blush should be differentiated from “papillary brush” seen at medullary sponge kidney. Abnormal papillary brush shows contrast fillings in abnormally dilated collecting tubules of renal medullae

## 2. Normal and Associated Findings: US of the Kidney

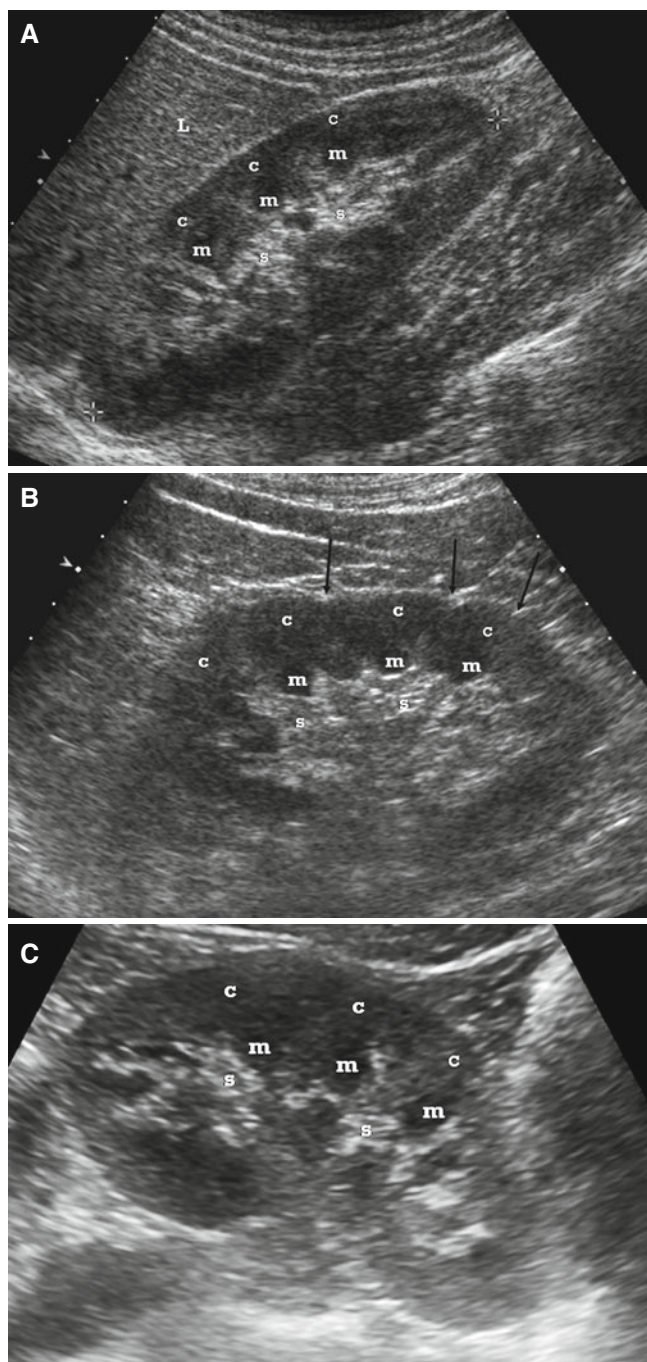


**Fig. 2.1** Normal grayscale US of the kidney. (A) Longitudinal US of the right kidney in a 37-year-old man shows normal echogenicity of the renal parenchyma. Note that the echogenicity of the renal cortex (*c*) is lower than that of the liver (*L*), and is higher than that of the renal medulla (*m*). (B) Longitudinal US of the left kidney in a 58-year-old man shows that renal cortical echogenicity (*c*) is slightly higher than that of the renal medulla (*m*). Note that the renal contour shows lobulations (*black arrows*). It is called fetal lobulation. (C) Longitudinal US of the left kidney in a 54-year-old woman shows renal cortex (*c*) and hypoechoic medulla (*m*). Note that corticomedullary differentiation is more prominent than A and B. *s* renal sinus

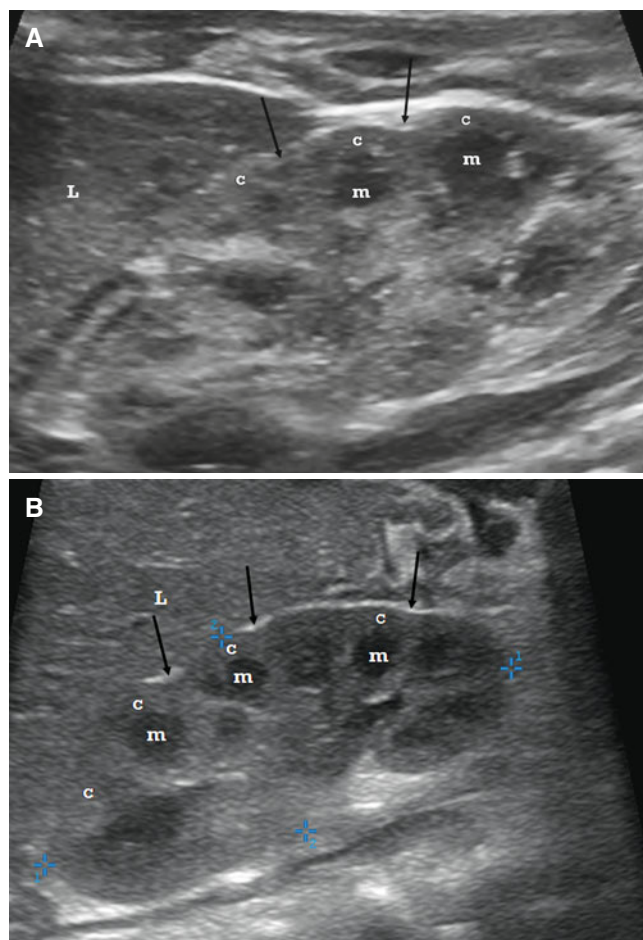


**Fig. 2.2** Normal grayscale US of the neonatal kidney. (A) Longitudinal US of the right kidney in a 1-day-old female infant shows relatively hyperechoic renal cortex (*c*) and prominent hypoechoic renal medulla (*m*). Note that the echogenicity of the normal renal cortex is higher than that of adult kidney and renal sinus fat echo is almost absent. *Black arrow* indicates fetal lobulation. (B) Longitudinal US of the right kidney in an 18-day-old woman infant. Note that the renal cortex shows relative hyperechogenicity and renal medulla shows prominent hypoechogenicity. *Black arrow* indicates fetal lobulation. *L* liver

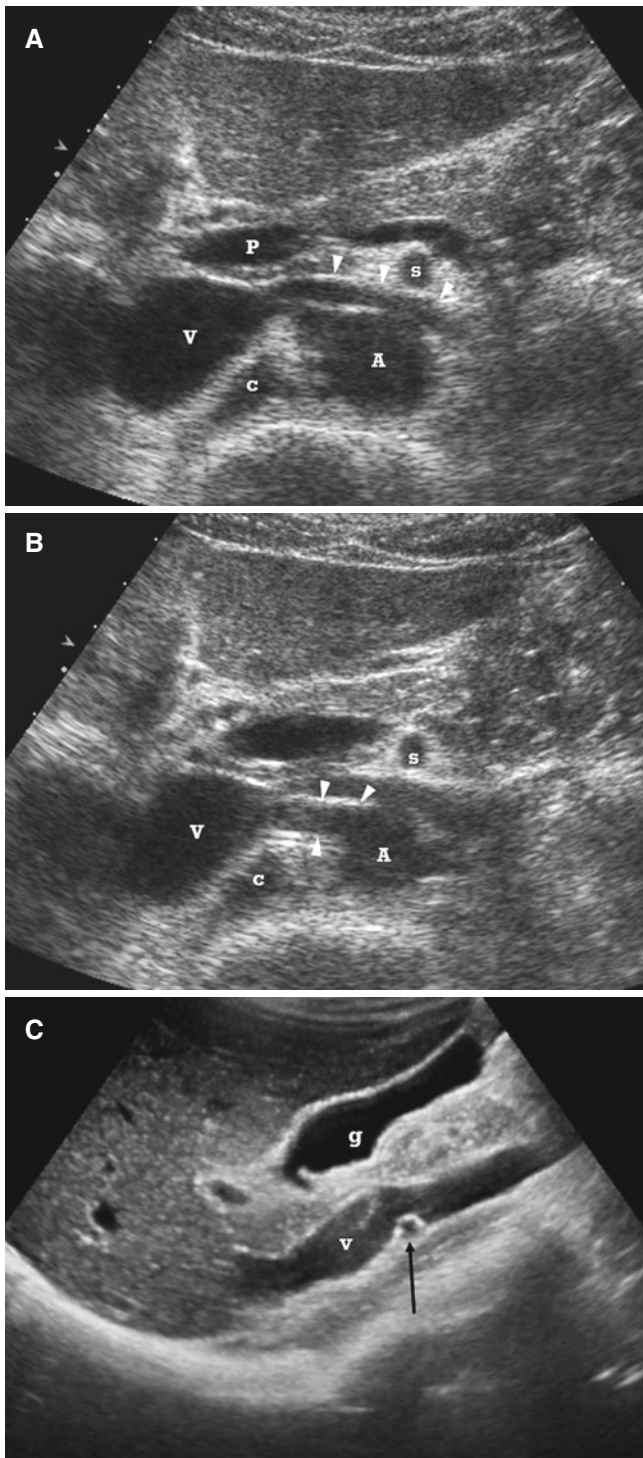


**Fig. 2.3** Grayscale US findings of the renal vessels: normal findings. (A) Transverse US in a 37-year-old man shows left renal vein (*white arrowheads*) coursing between the aorta (A) and superior mesenteric artery (s) to the inferior vena cava (V). (B) Transverse US in the same patient as A shows right renal artery (*white arrowheads*) arising from the aorta (A), V inferior vena cava. (C) Longitudinal US performed along the inferior vena cava (V) in a different patient shows right renal artery (*black arrow*) coursing behind the inferior vena cava. c crus of the diaphragm, G gall bladder, P portal vein, s superior mesenteric artery

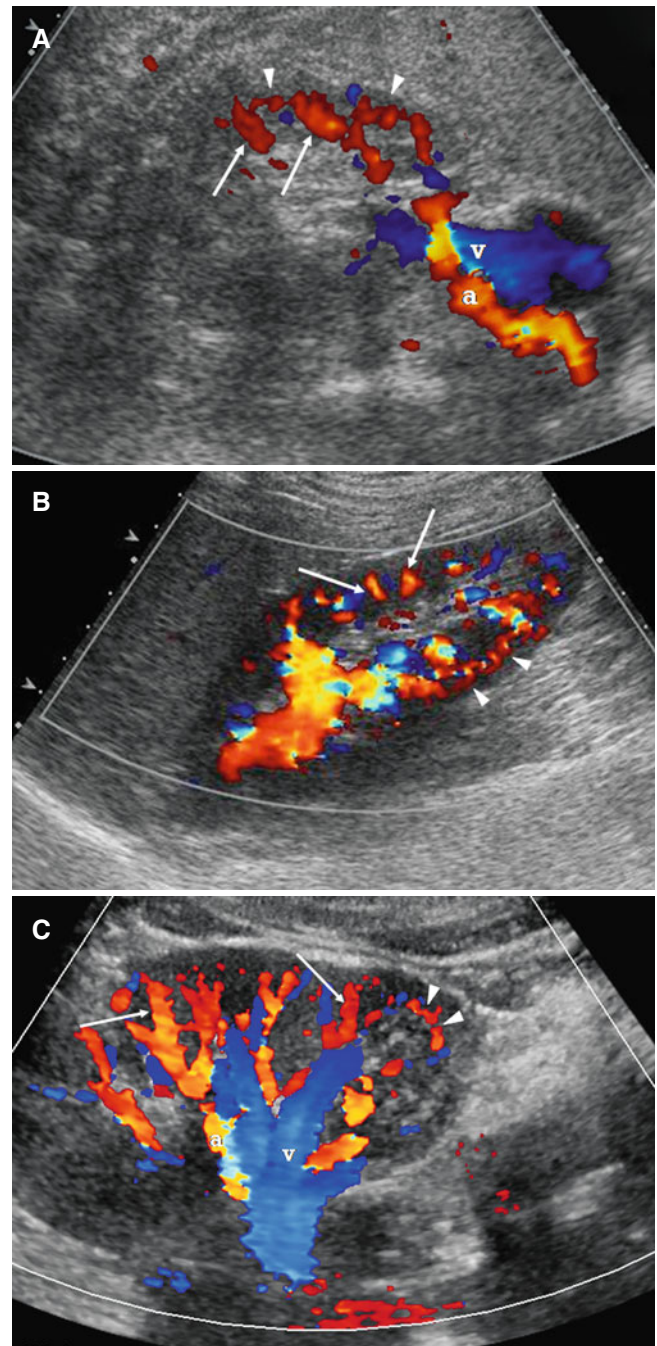


**Fig. 2.4** Color Doppler US findings of the renal vessels: normal findings. (A) Color Doppler US performed along the right renal vessels in a 51-year-old man shows right renal artery (a) and right renal vein (v). Also note intrarenal vessels including interlobar (*white arrows*) and arcuate (*white arrowheads*) vessels. (B) Color Doppler US of the right kidney in a 62-year-old woman well demonstrates intrarenal vessels including interlobar (*white arrows*) and arcuate vessels (*white arrowheads*). (C) Color Doppler US of the left kidney in a 27-year-old woman shows left renal artery (a) and right renal vein (v). Intrarenal vessels such as interlobar (*white arrows*) and arcuate (*white arrowheads*) vessels are also seen

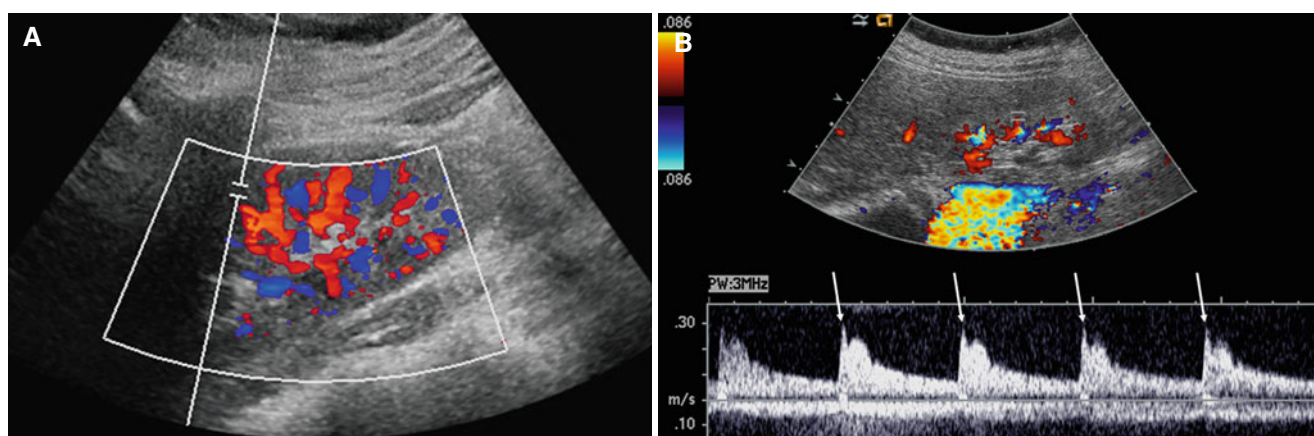


**Fig. 2.5** Spectral Doppler US findings of the intrarenal arteries: normal findings. (A) Spectral Doppler US of the right kidney performed at the level of interlobar artery in a 32-year-old woman shows normal Doppler spectral pattern with a resistive index of

0.63. (B) Spectral Doppler US of the right kidney performed at the level of interlobar artery in a 51-year-old woman shows normal spectral pattern with early systolic compliance peak (white arrows). Resistive index is 0.69 in this case

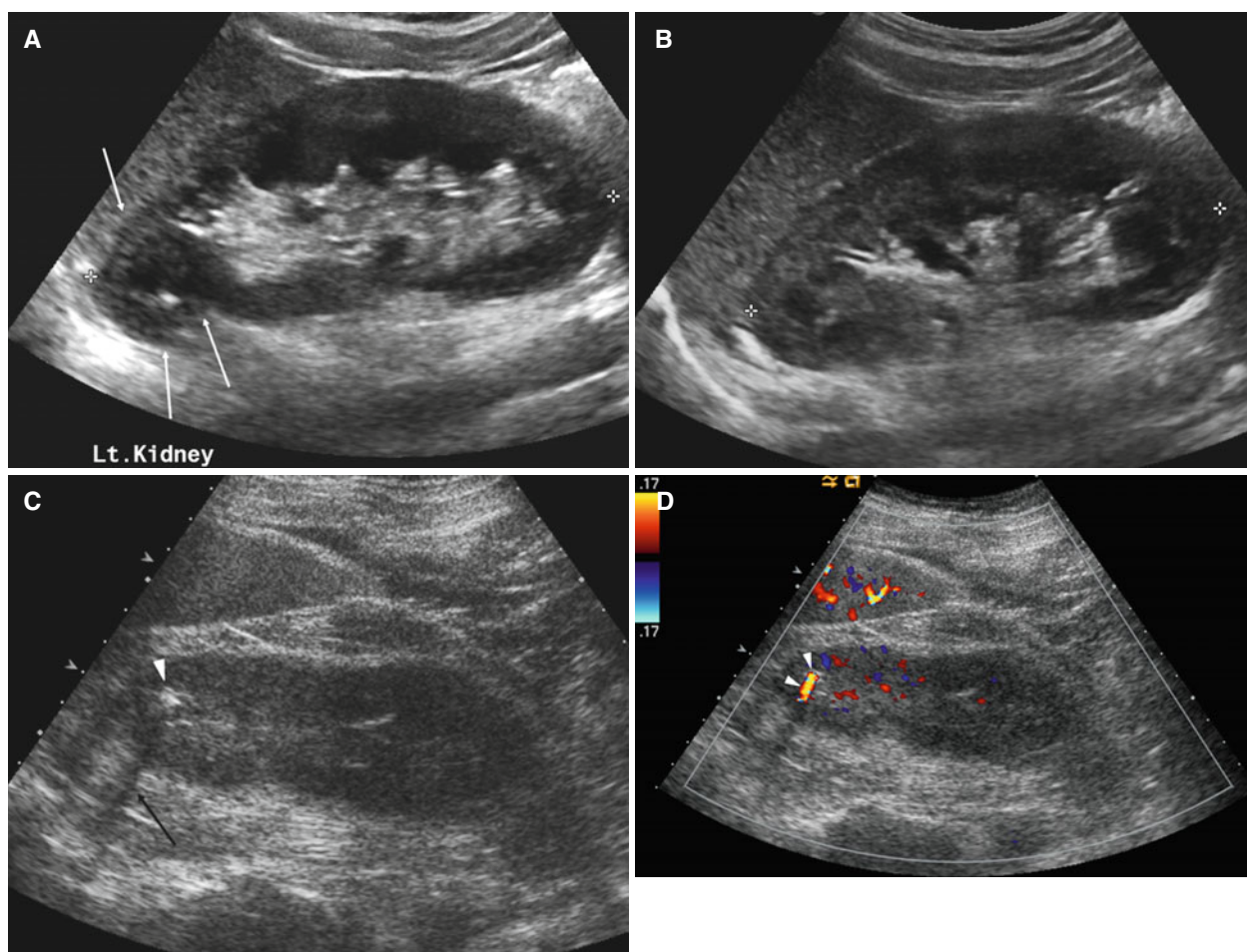


**Fig. 2.6** Duplication artifact and twinkling artifact. (A) Duplication artifact of the right kidney in a 26-year-old woman. Longitudinal US shows mass-like lesion in the upper pole (white arrows). This artifact is due to sound beam refraction between the lower pole of the spleen or liver and adjacent fat. (B) Longitudinal US of the same kidney as in A in a different angle shows no evidence of a mass in the upper pole. (C) Twinkling artifact of the right kidney in a 49-year-old man. Longitudinal

US shows an identified bright object (white arrowhead) with posterior shadowing (black arrow). (D) Color Doppler US in the same kidney as in C shows mixed color band (white arrowheads) with rapidly changing mixture of color behind a hyperechoic focus, probably caused by a papillary calcification or a small calyceal stone. It can be differentiated from true blood flow signal in that it has peculiar mixed color bands parallel to the US beam independent of arterial pulses

### 3. Normal Findings: CT of the Kidney

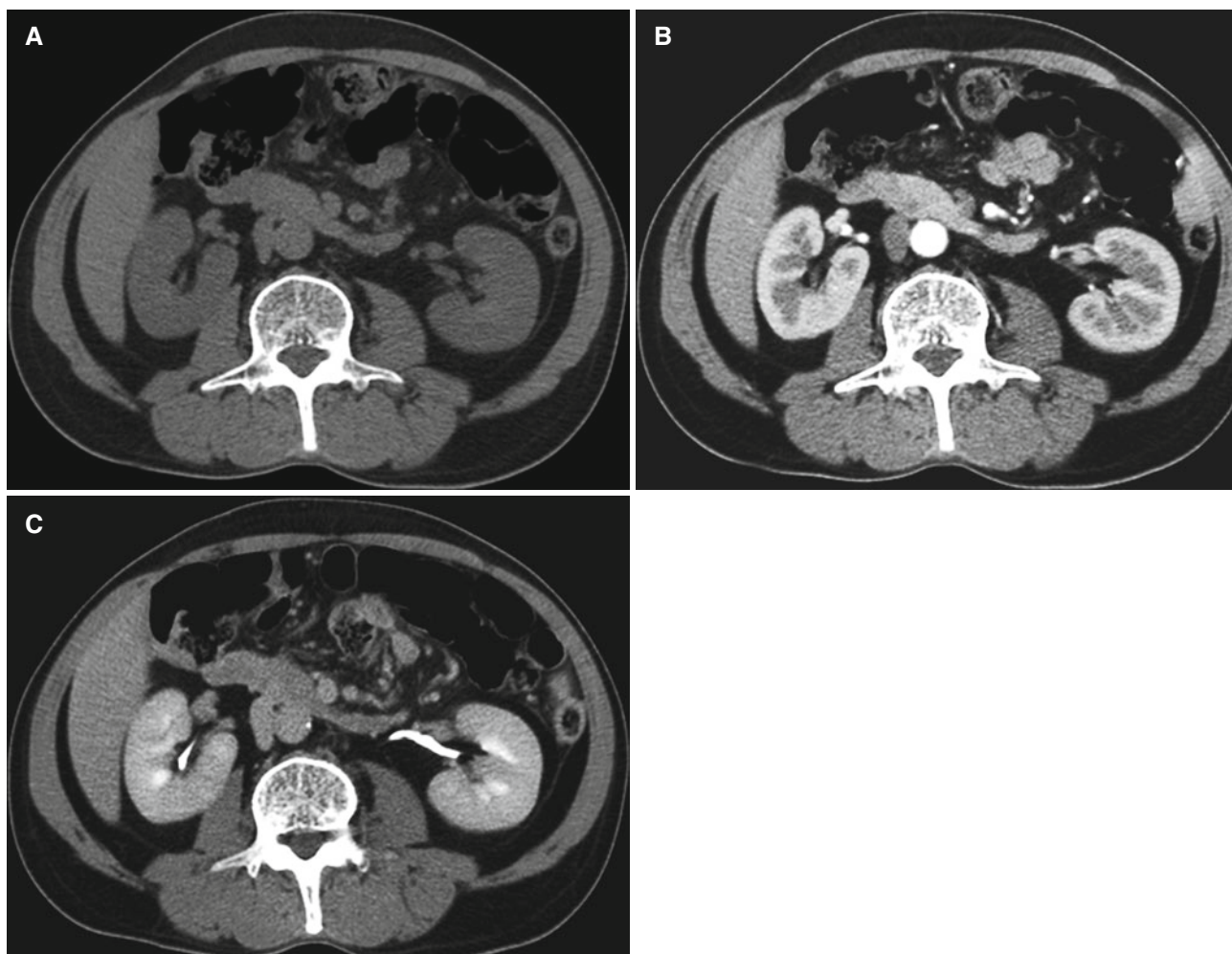


**Fig. 3.1** CT findings of the normal kidney in a 64-year-old man. (A) Nonenhanced CT shows smooth contour and homogeneous attenuation of the kidneys. (B) Contrast-enhanced CT in cortical phase shows strong enhancement of the renal cortex and low-attenuated renal medulla resulting in distinct corticomedullary differentiation. (C) CT scan in delayed excretory phase shows homogeneous enhancement of

the renal parenchyma and excreted contrast material in the renal pelvis. (D and E) Coronal and sagittal reformatted images are helpful to identify the anatomical location and the extent of the lesion. (F) Normal papillary blush on CT images. CT images show normal staining of renal papillae (*white arrowheads*) due to collection of contrast material in normal collecting ducts



**Fig. 3.1** (continued)

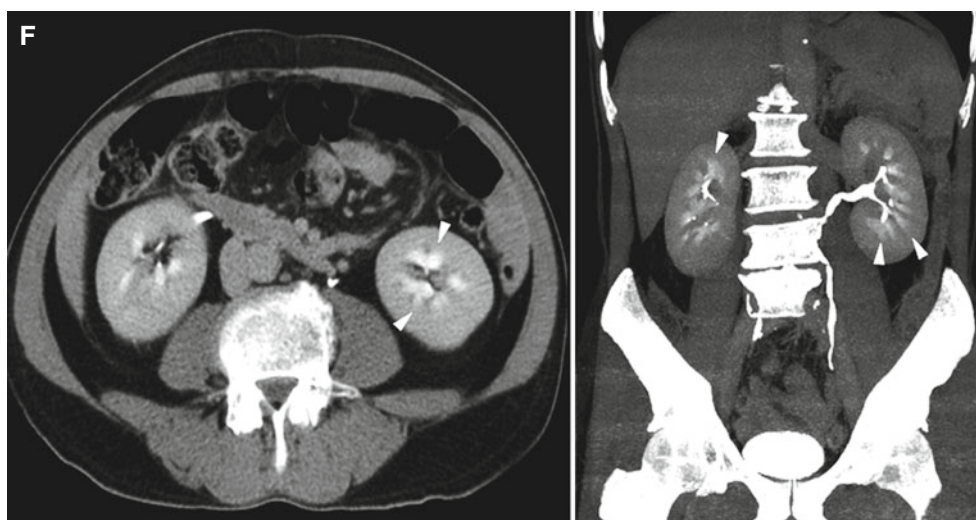


**Fig. 3.1** (continued)

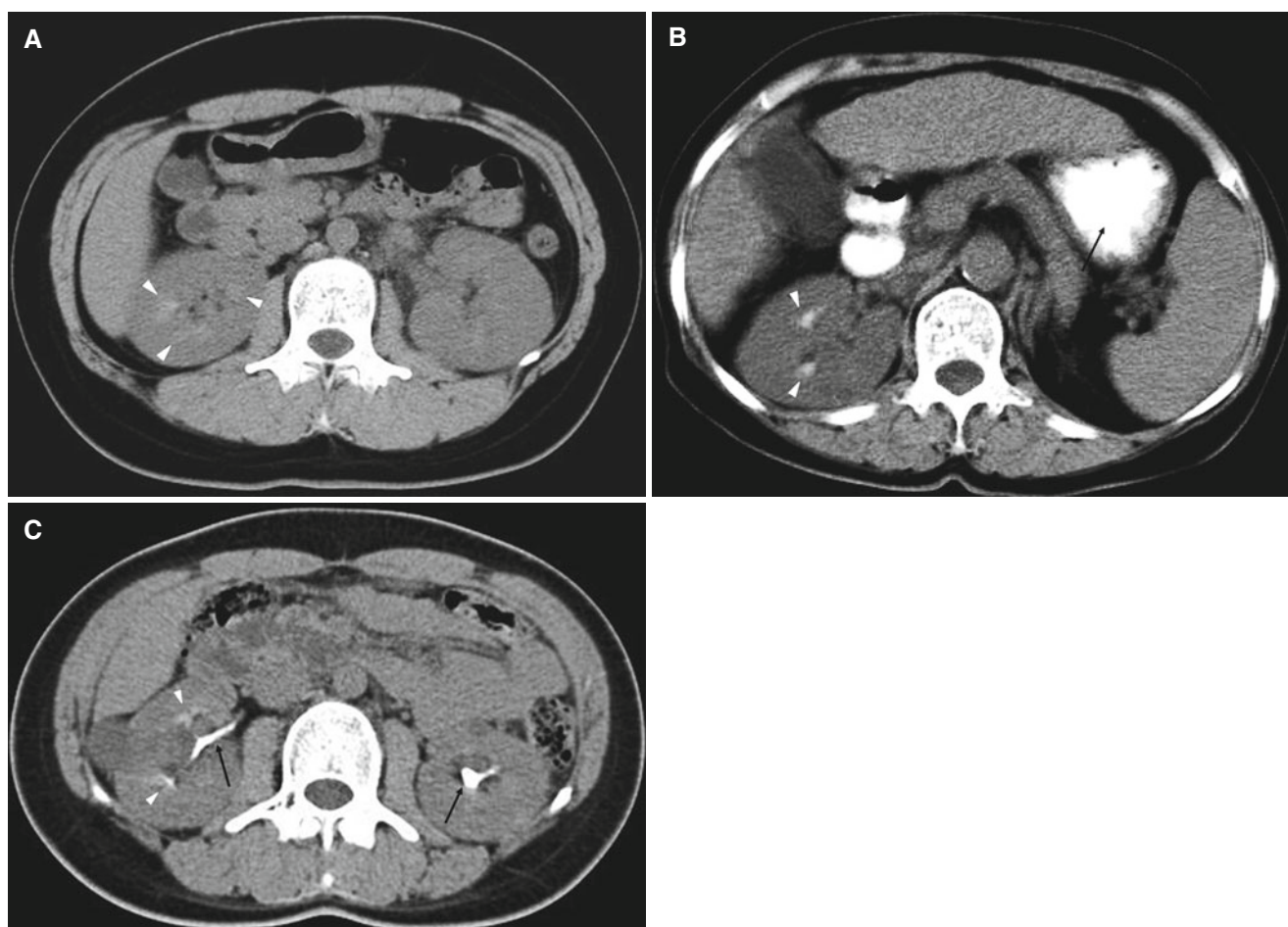


**Fig. 3.2** High attenuated renal medullae on nonenhanced CT. (A) Nonenhanced CT in a 26-year-old woman shows high attenuated medullae (*white arrowheads*) of the right kidney, probably due to dehydration. (B) Nonenhanced CT in a 72-year-old woman shows enhanced renal medullae (*white arrowheads*) of the right kidney. Note that stomach and duodenum are filled with high attenuated materials (*black*

*arrow*). Patient performed gastrointestinal study with diatrizoic acid. (C) Nonenhanced CT in a 29-year-old woman shows renal excretion of contrast material in the both pelvocaliceal system (*black arrows*). Note faintly enhanced renal medullae of right kidney (*white arrowheads*). Patient performed MRI with contrast-enhancement (gadolinium-based MR contrast material) before CT scanning

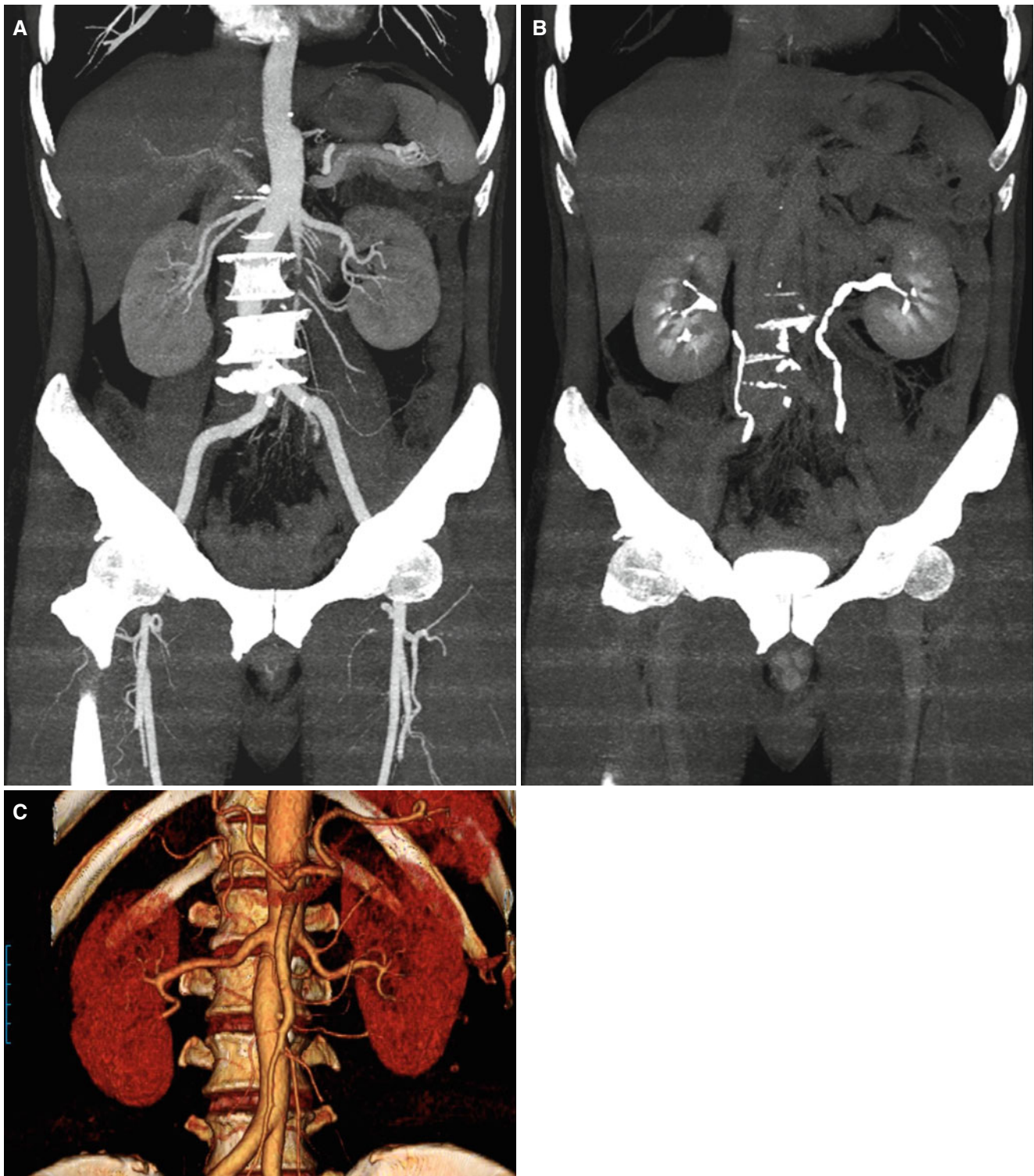


**Fig. 3.3** CT images using postprocessing techniques. (A and B) Maximum-intensity projection (MIP) images show entire renal arteriogram and urograms in a 64-year-old man. Note obliteration of iliac

arteries by high-density pelvic bony shadows on A. (C) Three-dimensional volume-rendered image demonstrates good presentation of branches from abdominal aorta

#### 4. Normal Findings: MRI of the Kidney

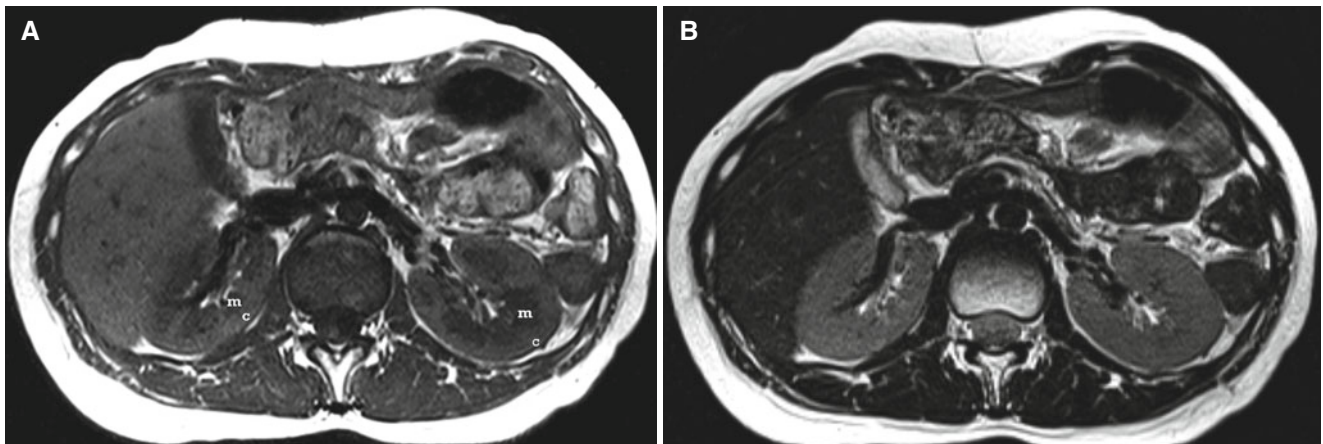


**Fig. 4.1** Normal turbo spin-echo MR images of the kidney in a 67-year-old woman. **(A)** T1-weighted turbo spin-echo MRI (repetition time [TR]/echo time [TE]=490/8.3 ms; flip angle=150°) shows distinct corticomedullary contrast demonstrated by high intensity of the

renal cortex (*c*) and low intensity of the renal medulla (*m*). **(B)** On T2-weighted turbo spin-echo MRI (TR/TE=2,500/98 ms; flip angle=150°), the signal intensities of the renal cortex and medulla are increased, and they are not differentiated

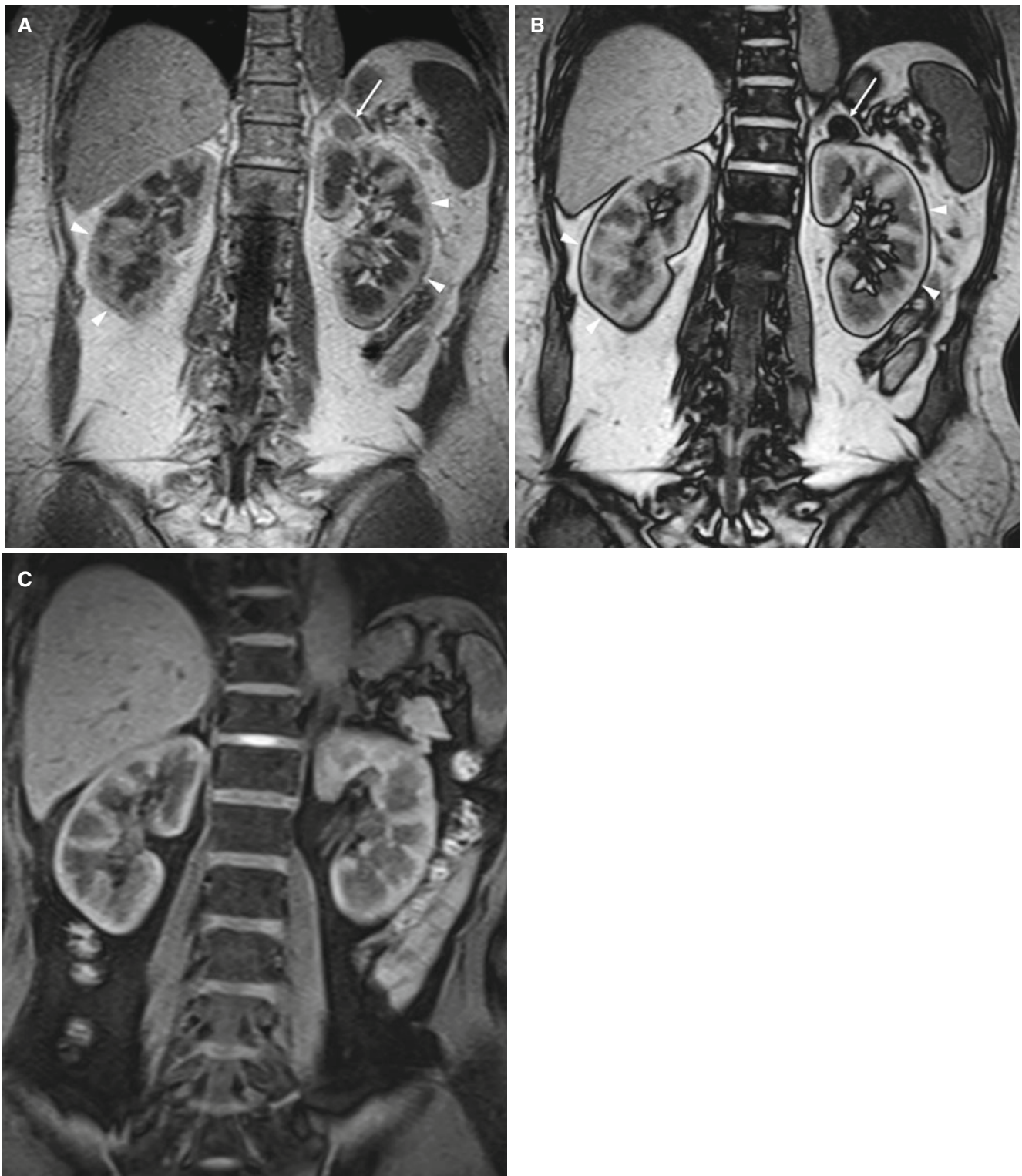


**Fig. 4.2** Advanced MRI techniques such as chemical-shifting imaging and fat-suppression imaging in a 67-year-old woman. The in-phase (A) (TR/TE=110/5.0 ms; flip angle=70°) and opposed phase (B) (TR=110/2.4 ms; flip angle=70°) gradient echo images show signal drop of left adrenal mass (*white arrow*) suggesting adrenal adenoma. Note that dark outlining (*white arrowheads*) between kidney and surrounding fat is prominent on opposed phase image.

In- and opposed-phase techniques show decrease in signal (signal drop) from voxels containing both water and fat. Using these techniques, it is possible to detect the microscopic, intravoxel lipid. (C) The fat-suppression T1-weighted gradient echo MRI using volume interpolate breath-hold gradient echo sequence (VIBE) (TR/TE=4.8/2.3 ms; flip angle=10°) shows improvement of tissue contrast between kidney and adjacent fat

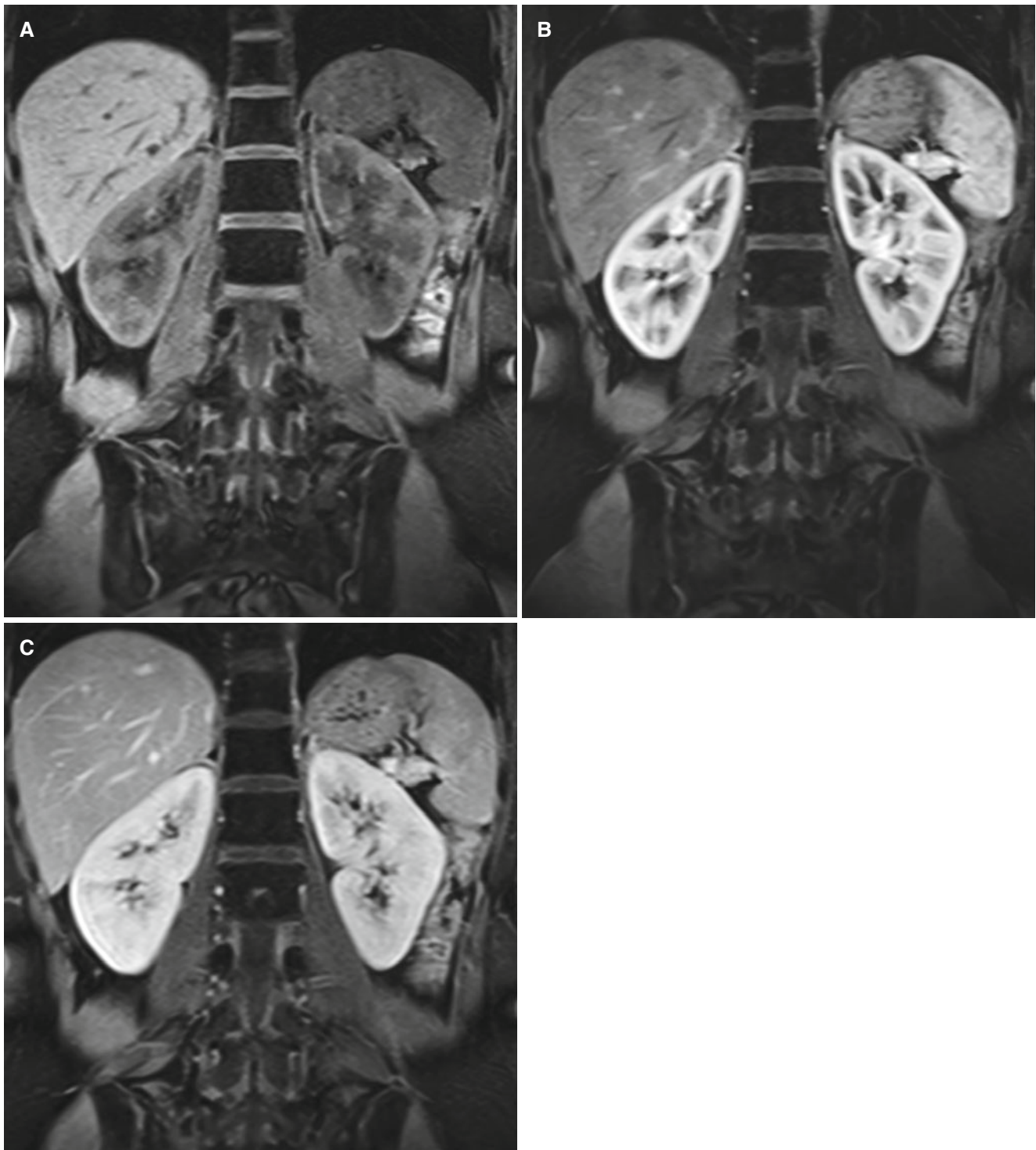


**Fig. 4.3** Normal fat-suppressed contrast-enhanced T1-weighted gradient-echo MRI using VIBE (TR/TE=4.8/2.3 ms; flip angle=10°) in a 30-year-old woman. (A) Nonenhanced T1-weighted coronal MRI shows improved tissue contrast due to fat suppression. Note normal signal intensity of the renal parenchyma with visible corticomedullary

contrast. (B) Contrast-enhanced MRI obtained 1-min after injection of contrast material shows enhancement of the renal cortex with distinct corticomedullary contrast. (C) MRI obtained 3-min after injection of contrast material shows similar degree of enhancement of the renal cortex and medulla

## 5. Variations of Renal Position



**Fig. 5.1** The right kidney higher than the left kidney in a 53-year-old woman with liver cirrhosis and splenomegaly. A 15-min IVU shows higher right kidney and lower left kidney because of shrunken liver and splenomegaly due to liver cirrhosis

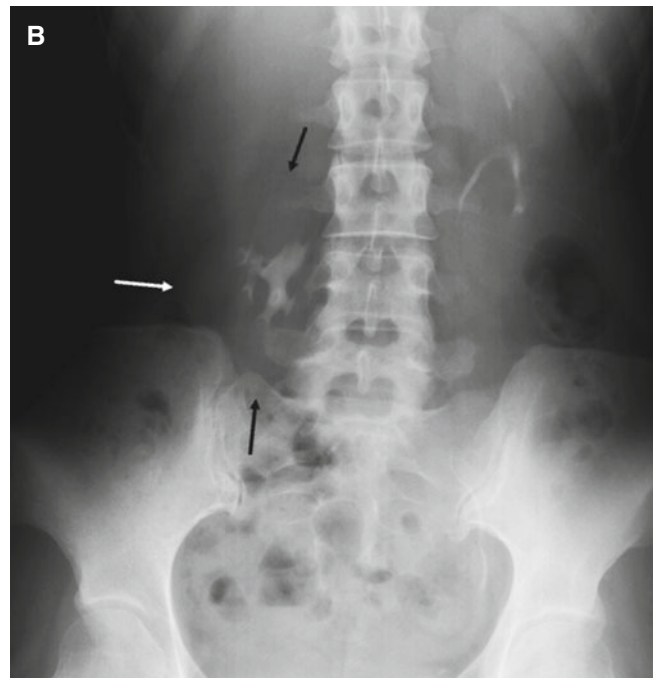
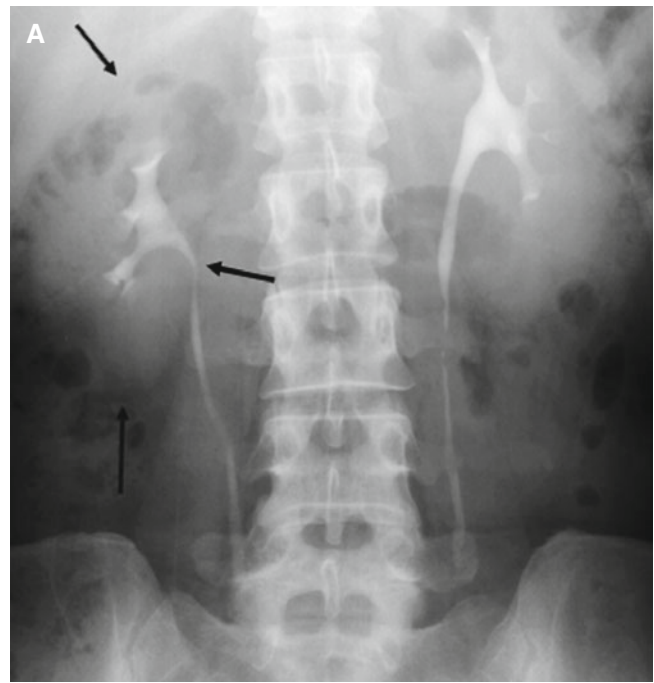


**Fig. 5.2** Nephroptosis on IVU. (A) Nephroptosis in a 41-year-old woman. IVU in supine position shows normal position of the right kidney (*black arrows*). (B) In erect position, the right kidney displaces downward (*white and black arrows*) to the degree of two lumbar vertebral heights

**Fig. 5.3** Nephroptosis in a 50-year-old woman. IVU in erect position shows low position of the right kidney (*arrows*). The right ureter has normal length and so is tortuous (*black arrowheads*)



## 6. Various Appearances of the Renal Pelvis and Calyx



**Fig. 6.1** Various shapes of the renal pelvis on IVU. IVU shows two typical shapes of normal renal pelvis: a funnel-shaped pelvis on left kidney (*black arrow*) and a box-shaped pelvis on the right kidney (*curved black arrow*)

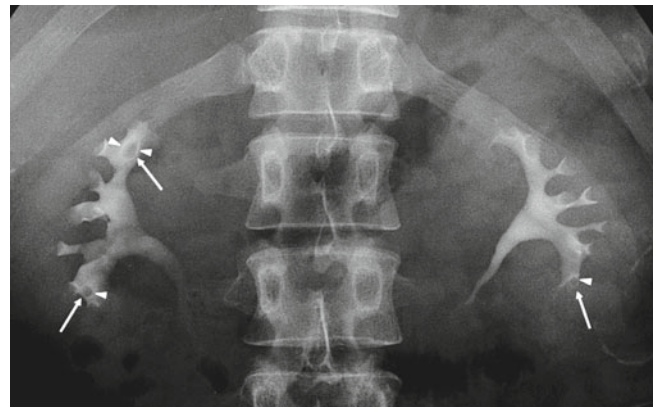


**Fig. 6.3** Prominent end-on papilla mimicking a calyceal-filling defect in a 30-year-old man. A 15-min IVU shows round radiolucencies (*white arrows*) in the upper polar calyx of right kidney and the lower polar calyces of both kidneys due to prominent end-on papillae. These radiolucencies may mimic urothelial tumors or blood clots. Note that the radiolucencies are surrounded by thin ringlike radio-opacities (*white arrowheads*) that represent contrast material in the calyceal fornices

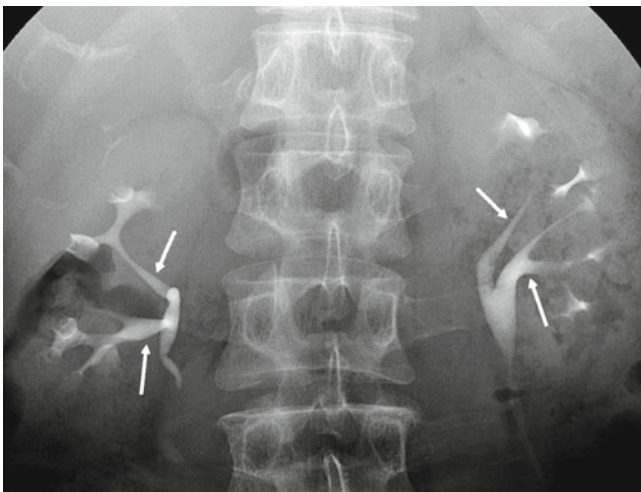


**Fig. 6.2** Bifid pelvis in a 66-year-old man. A 15-min IVU shows bifid pelvis (*white arrows*) of both kidneys separated by invaginated renal parenchyma. This is the mildest form of duplication anomaly of the renal pelvis and ureter

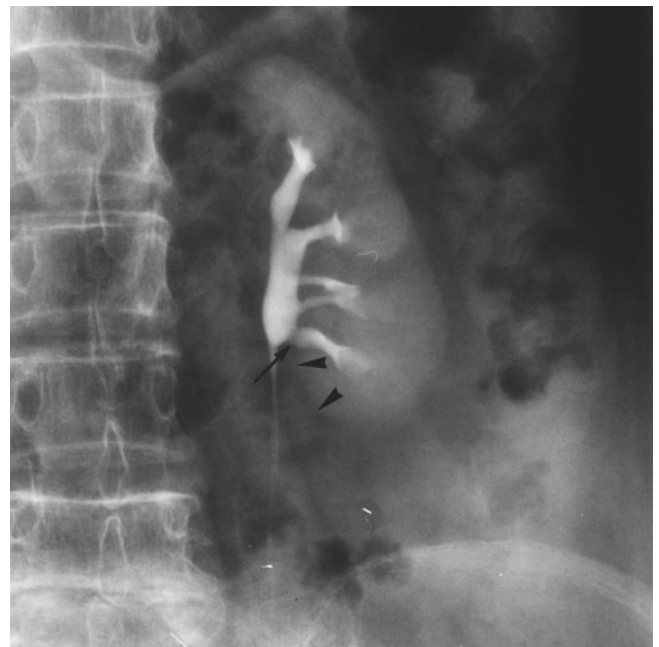


**Fig. 6.4** Extrarenal calyx in a 67-year-old woman. IVU shows an elongated left renal pelvis, which is mainly extrarenal in location. Note that the infundibulum of the lower polar calyx (*black arrow*) is located outside of the lower medial margin of the left kidney (*black arrowheads*)

## 7. Vascular Indentations on the Urinary Tract

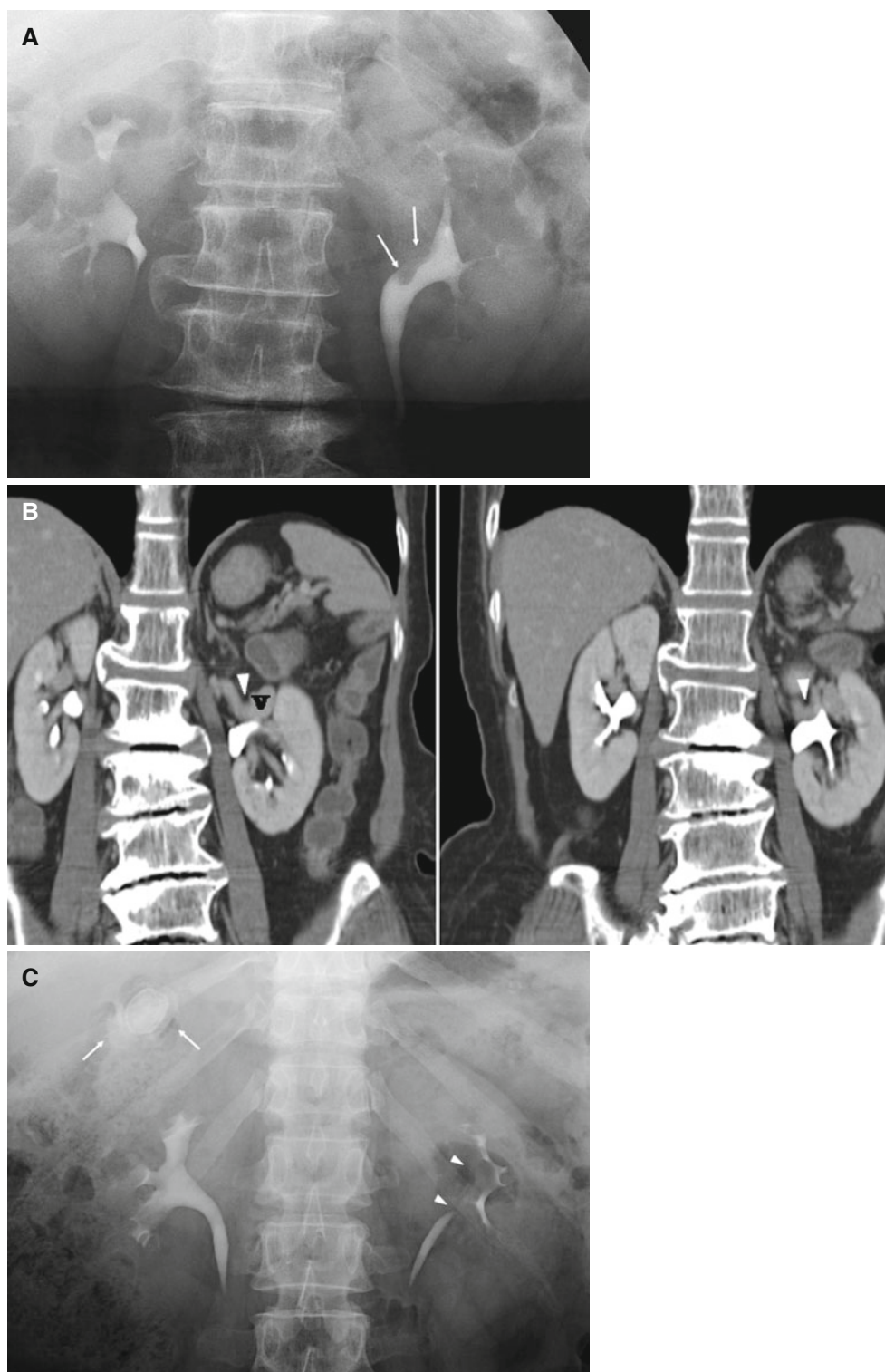


**Fig. 7.1** Vascular indentations on IVU and CT. (A) 5-min IVU in a 67-year-old woman shows clear margined filling defect (*white arrows*) at superior aspect of the left renal pelvis. (B) Contrast-enhanced CT with coronal reformation images in the same patient as A show compressing renal veins (*white arrowheads*; v). (C) 5-min IVU in a 60-year-old

woman shows vascular indentation (*white arrowheads*) of left renal pelvocalyces. *White arrows* indicate gall bladder stone. (D) Contrast-enhanced CT with coronal reformation images in the same patient as C shows compressing left renal veins (*white arrows*)

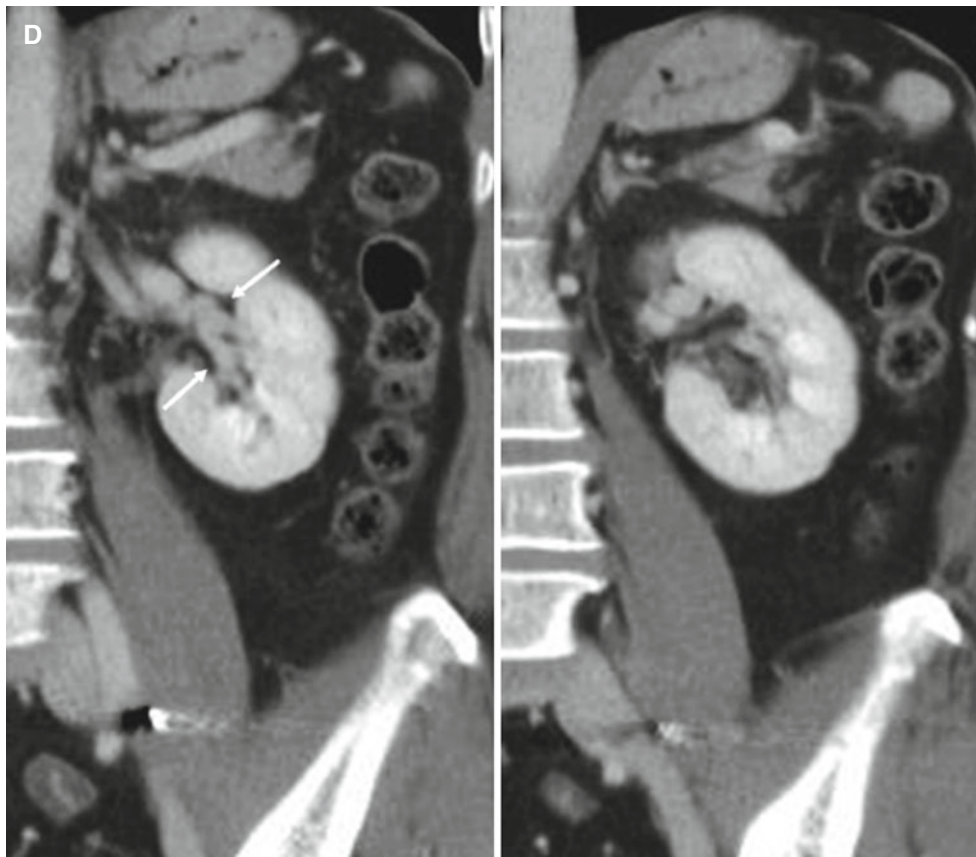


**Fig. 7.1** (continued)

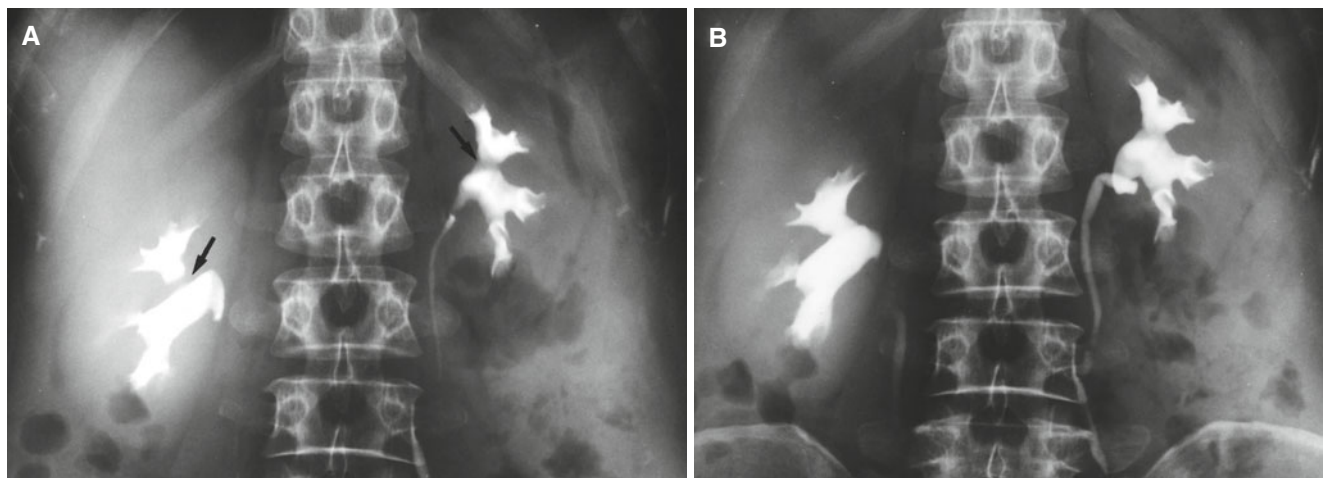


**Fig. 7.2** Vascular indentations on the calyceal infundibulum in a 52-year-old woman with intermittent flank pain. (A) IVU obtained 25 min after injection of contrast material shows well-defined linear

impressions (*black arrows*) on the upper calyceal infundibuli of both kidneys. (B) The vascular impressions were less well-demonstrated on a 15-min IVU

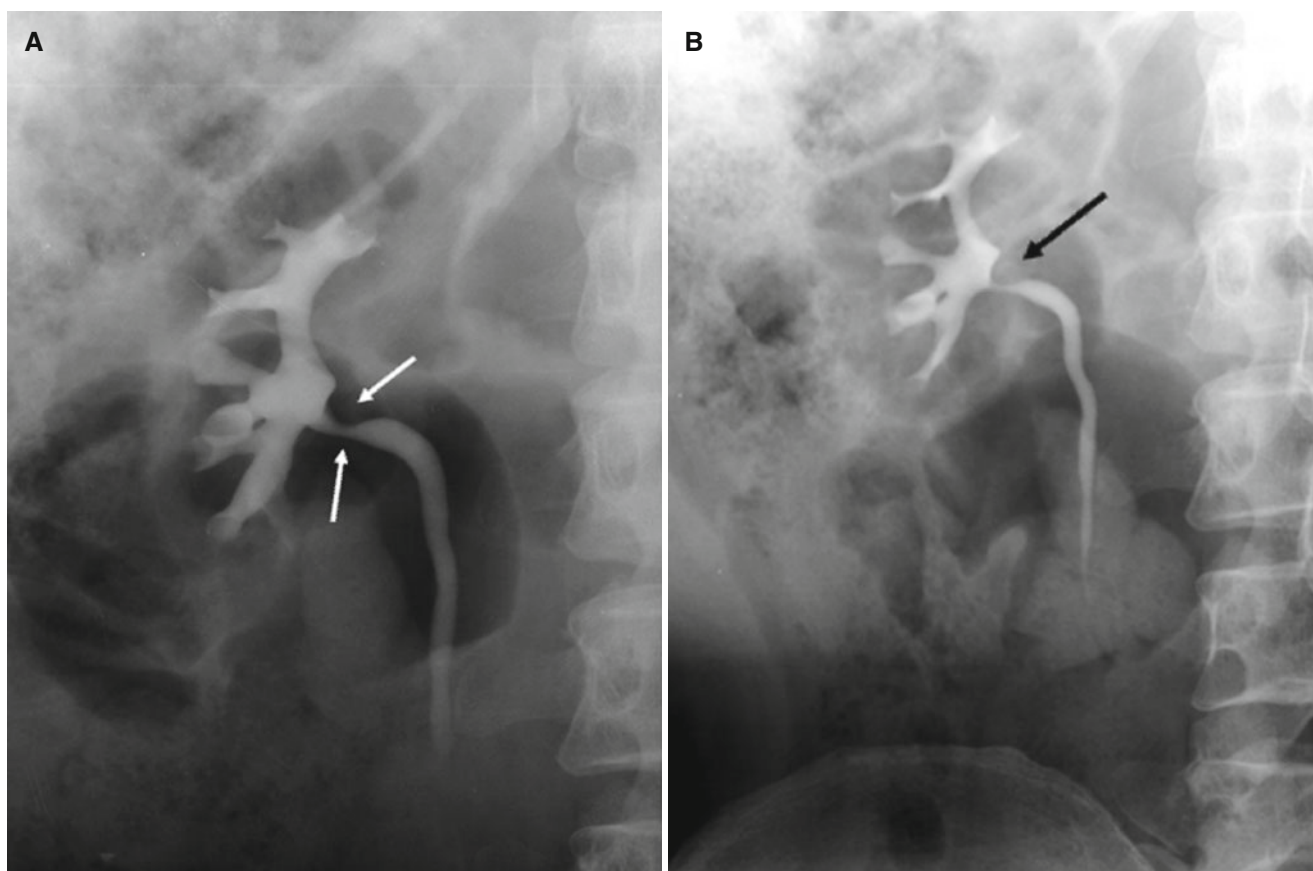


**Fig. 7.3** Arterial indentation on the renal pelvis of the right kidney in a 62-year-old man. (A and B) 5- and 15-min IVU images show persistent well-defined arterial impressions (*arrows*) on the right renal pelvis

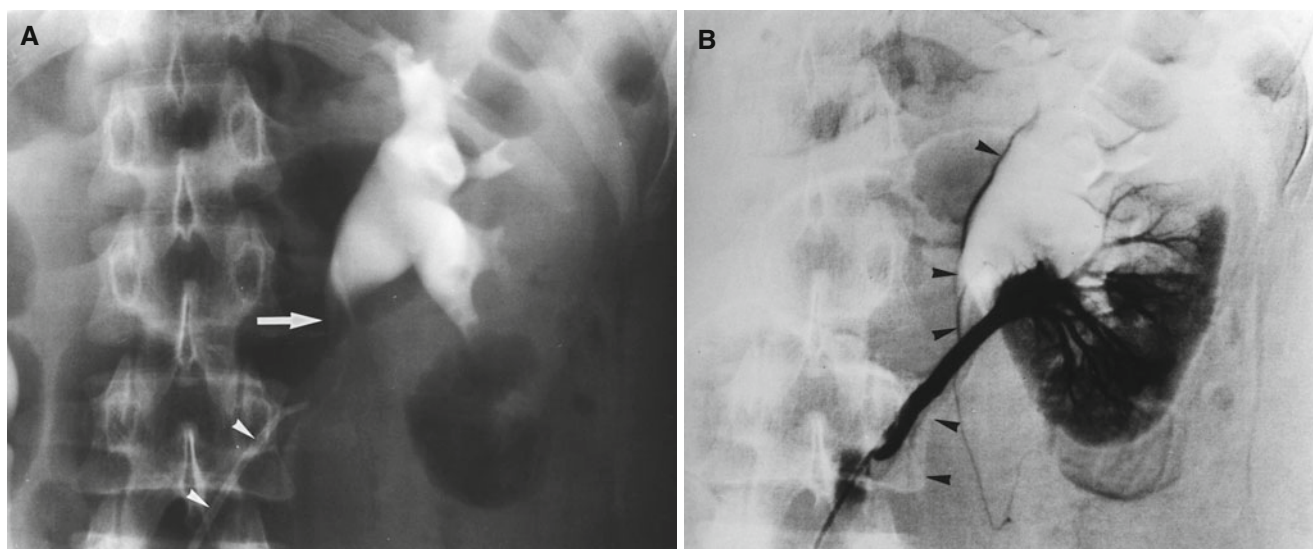


**Fig. 7.4** Impression on the right ureteropelvic junction by an accessory renal artery to the lower pole of the left kidney in a 50-year-old woman. (A) IVU obtained before arteriography shows slight dilatation of the left renal pelvis and narrowing of the ureteropelvic junction (*white arrow*). Note a catheter in the accessory lower-polar artery (*white*

*arrowheads*). (B) Selective arteriography of the accessory lower-polar artery demonstrates the relation of the artery and the urinary tract. Note that the renal pelvis and proximal ureter that are filled with contrast material appear as bright shadow (*black arrowheads*) on this digital subtraction arteriogram

## 8. Renal Backflows

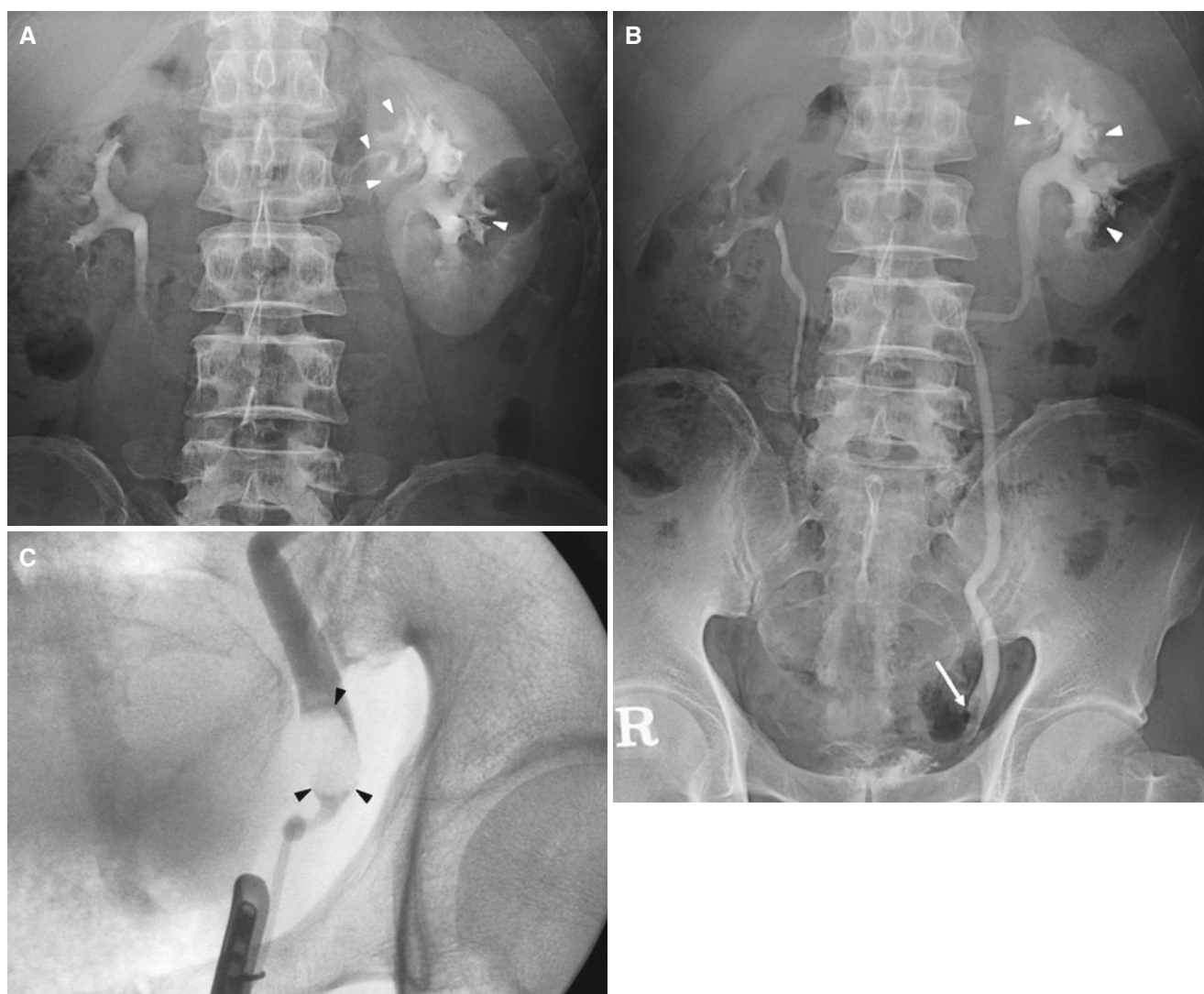
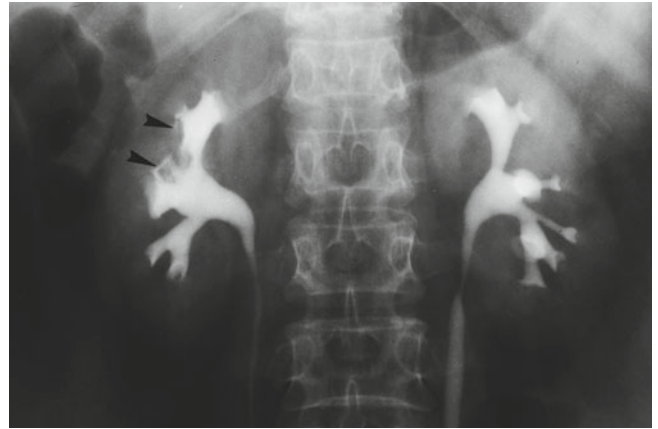


**Fig. 8.1** Pyelosinus backflow demonstrated on IVU in a 60-year-old man with ureteral tumor. (A) 15-min IVU shows hydronephrosis of left kidney with delayed contrast excretion. Multifocal contrast leak from the upper and lower polar calyces to the renal sinus are seen (*white arrowheads*), probably due to forniceal rupture. (B) 60-min IVU shows

persistent hydronephrosis and hydroureter. Residual leak of contrast material is seen (*white arrowhead*). Note a filling defect (*white arrow*) at distal level of left ureter due to ureteral tumor. (C) Retrograde urography shows a round filling defect (*black arrowheads*) representing ureter tumor at left distal ureter

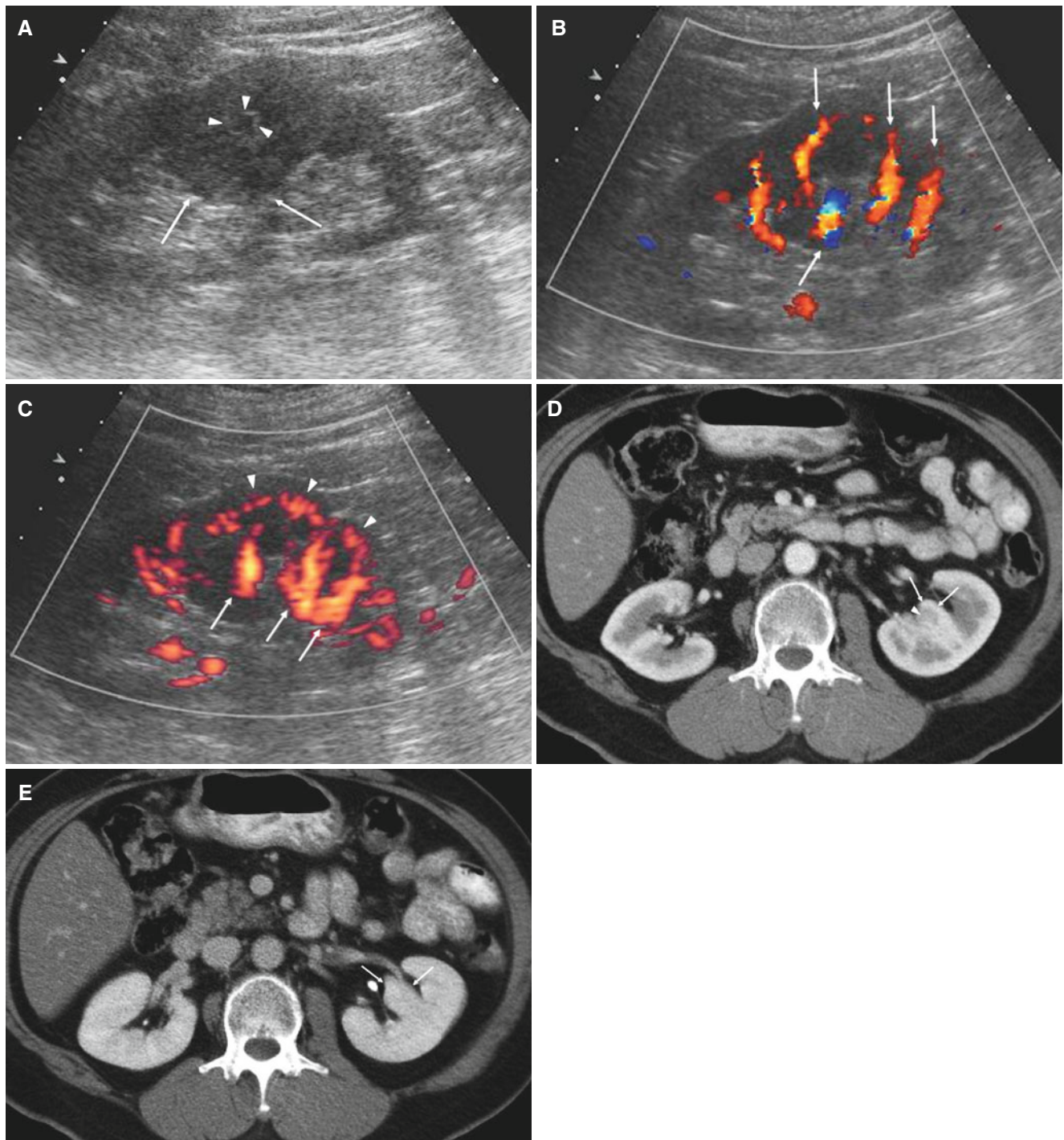


**Fig. 8.2** Forniceal rupture due to ureteral obstruction by ureter stone in a 50-year-old woman. A 15-min IVU shows leak of contrast material (*white arrowheads*) from the calyceal fornix in the lower polar area of the right kidney



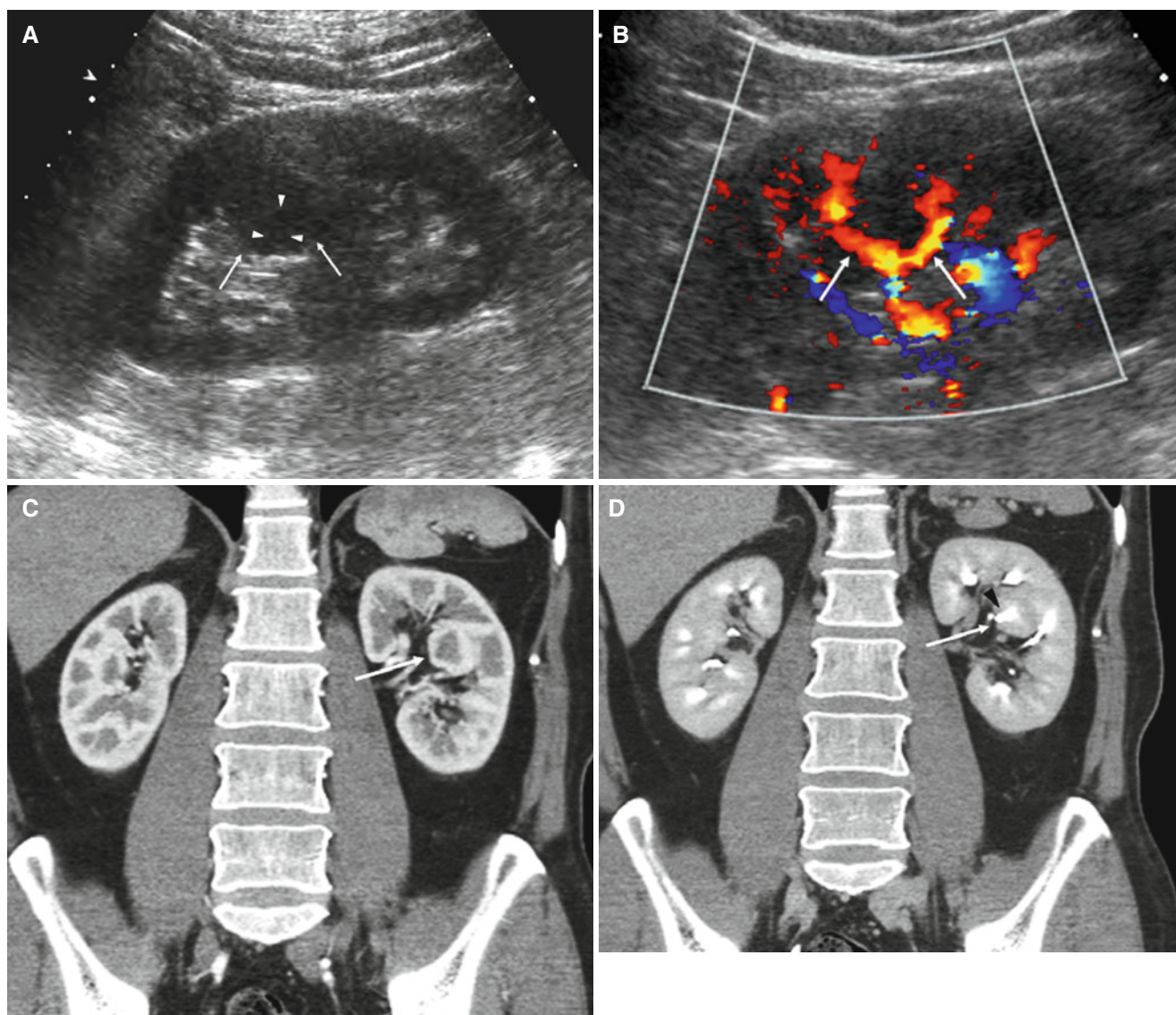
**Fig. 8.3** Calyceal rupture due to ureteral compression during IVU. A 15-min IVU shows leak of contrast material (*black arrowheads*) from the calyceal fornix in the upper pole area of the right kidney. This patient does not have ureteral obstruction and this leakage of contrast material is probably due to rupture of calyceal fornix caused by ureteral compression applied during IVU

## 9. Renal Pseudotumors



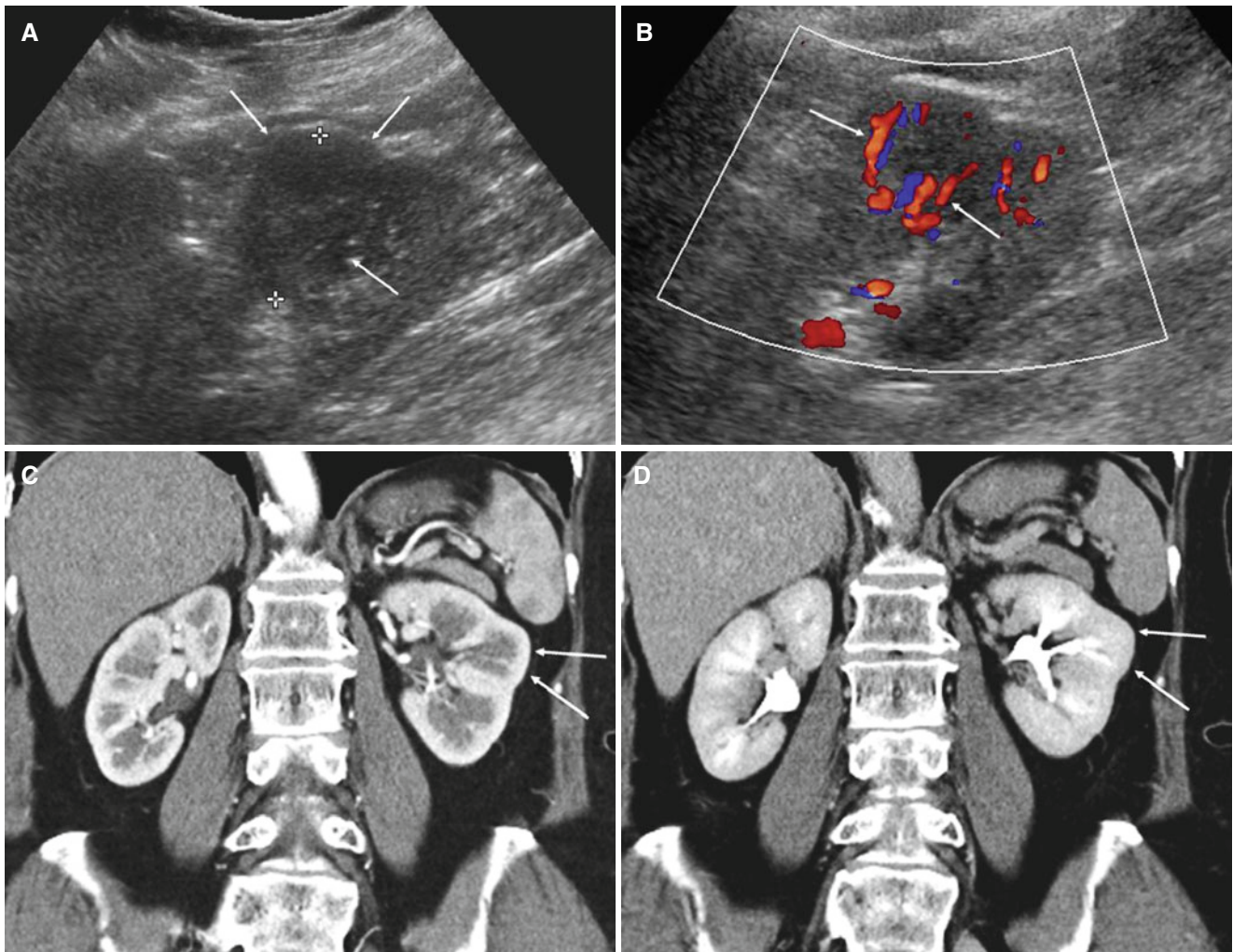
**Fig. 9.1** Prominent column of Bertin of the left kidney in a 69-year-old woman. (A) Longitudinal US shows a prominent column of renal parenchyma (*white arrows*) projecting into the renal sinus. The column contains a focal hypoechoic area (*white arrowheads*) that probably represents a medulla surrounded by septal cortical tissues. (B and C) Color and Power Doppler US images show interlobar vessels running through the column (*white arrows*) and arcuate vessels (*white arrowheads*)

within the column. (D and E) Contrast-enhanced CT in corticomedullary phase shows a prominent column (*white arrows*) projecting into the renal sinus. Contrast enhancement of the column is identical to that of the adjacent renal parenchyma. Note that the column contains a medulla (*white arrowhead* in D) that is less enhanced than cortex at corticomedullary phase CT



**Fig. 9.2** Prominent column of Bertin of left kidney in a 60-year-old man. (A) Longitudinal US shows a prominent column of renal parenchyma (white arrows) projecting into the renal sinus. The column contains a focal hypoechoic area (white arrowheads) that probably represents a medulla surrounded by septal cortical tissues. (B) Color Doppler US shows interlobar vessels (white arrows) running through the column. (C) Contrast-enhanced CT with coronal reformation in corticomedullary

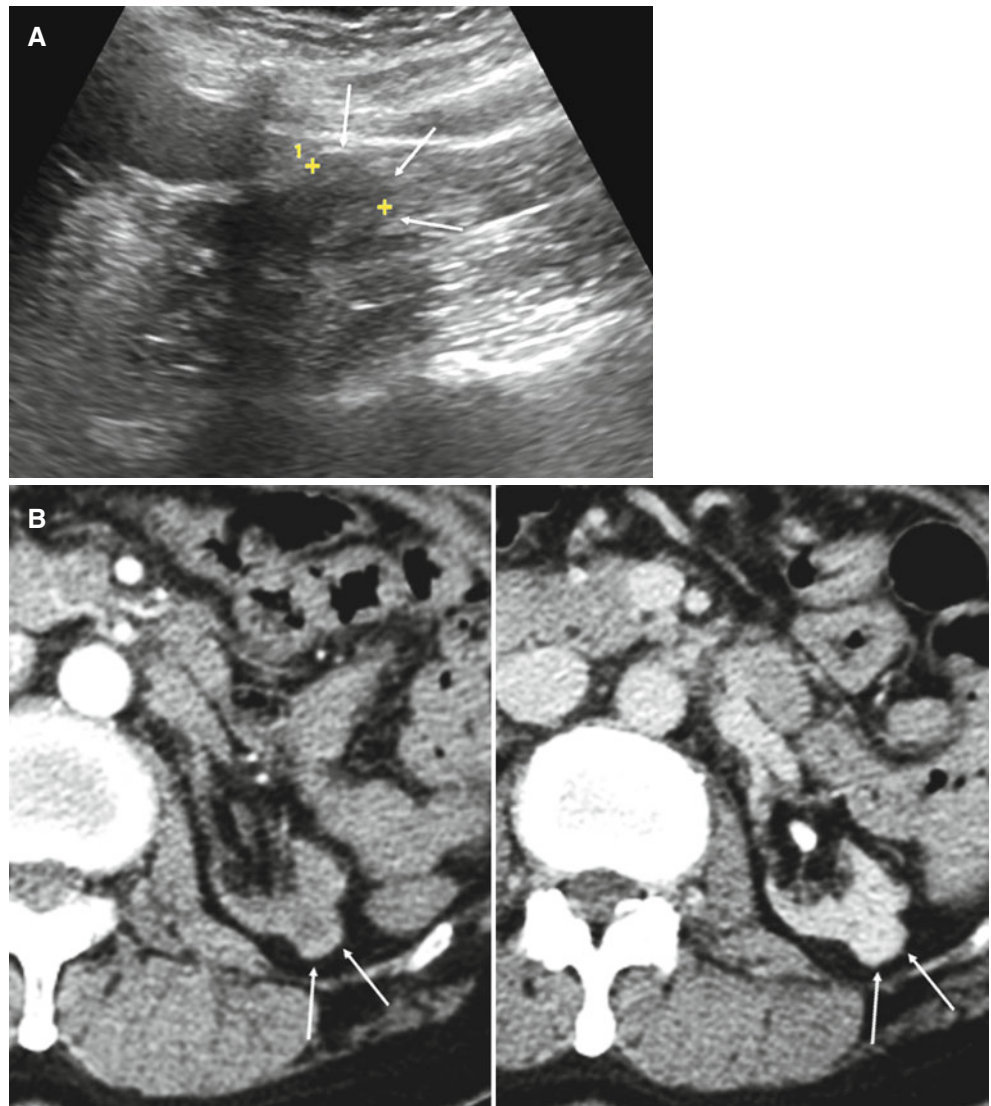
phase shows a column (white arrow) projecting into the renal sinus. Contrast enhancement of the prominent column is identical to that of the adjacent renal parenchyma. (D) Contrast-enhanced CT with coronal reformation in excretory phase shows a prominent column (white arrow) projecting into the renal sinus. Note that the column contains a medulla with excretion into a calyx (black arrowhead)



**Fig. 9.3** Dromedary (splenic) hump in a 58-year-old woman. (A) Longitudinal US shows a bulging contoured low echoic lesion on the lower lateral border of the left kidney (*white arrows*). (B) Color Doppler US shows vascular flow signals passing through the lesion (*white*

*arrows*). (C and D) Contrast-enhanced coronal reformatted CT images show a focal bulging of parenchymal tissue (*white arrows*) without demonstrable mass on the lateral border of the left kidney

**Fig. 9.4** Localized compensatory parenchymal hypertrophy of renal parenchyma in a 51-year-old woman with end-stage kidney disease kidney. **(A)** Longitudinal US shows an exophytic round nodular mass-like lesion (white arrows, marker '+') in lower pole of small-sized left kidney. **(B)** Dynamic contrast-enhanced CT images reveal exophytic round parenchymal tissue that shows similar contrast enhancement to adjacent normal parenchyma (white arrows). Left kidney shows severe atrophic change with localized compensatory parenchymal hypertrophy that may be mistaken for an exophytic renal tumor



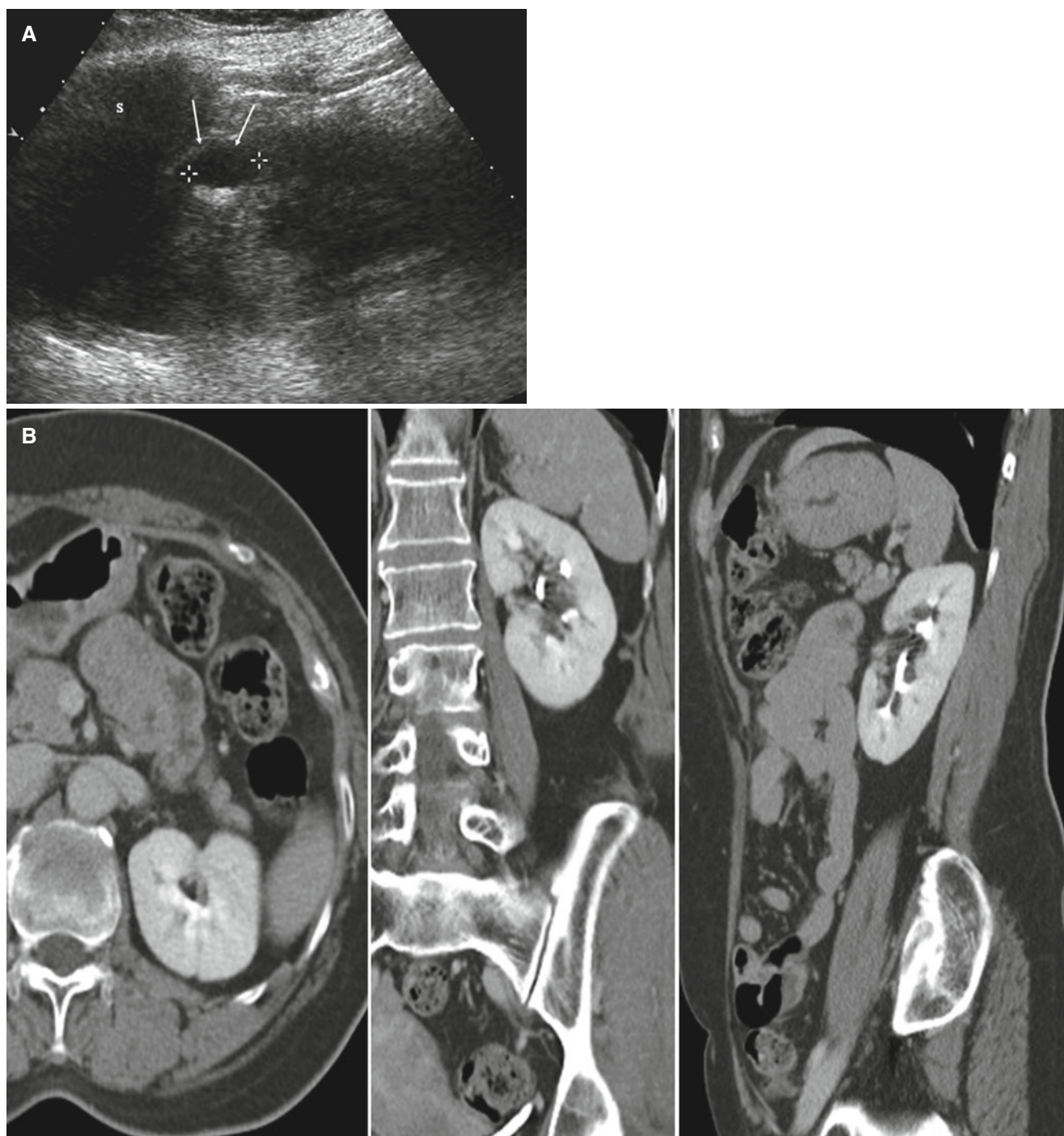


**Fig. 9.5** Renal pseudotumor due to duplication artifact in a 52-year-old woman. **(A)** Longitudinal US images show round hypoechoic lesion (*white arrows*) with thick echogenic wall in the interpolar area. On US, it was diagnosed as a complicated cyst. *S* spleen. **(B)** Contrast-enhanced

CT shows no demonstrable cystic lesion. This pseudolesion is probably due to duplication artifact caused by beam refraction between the lower pole of the spleen and adjacent fat

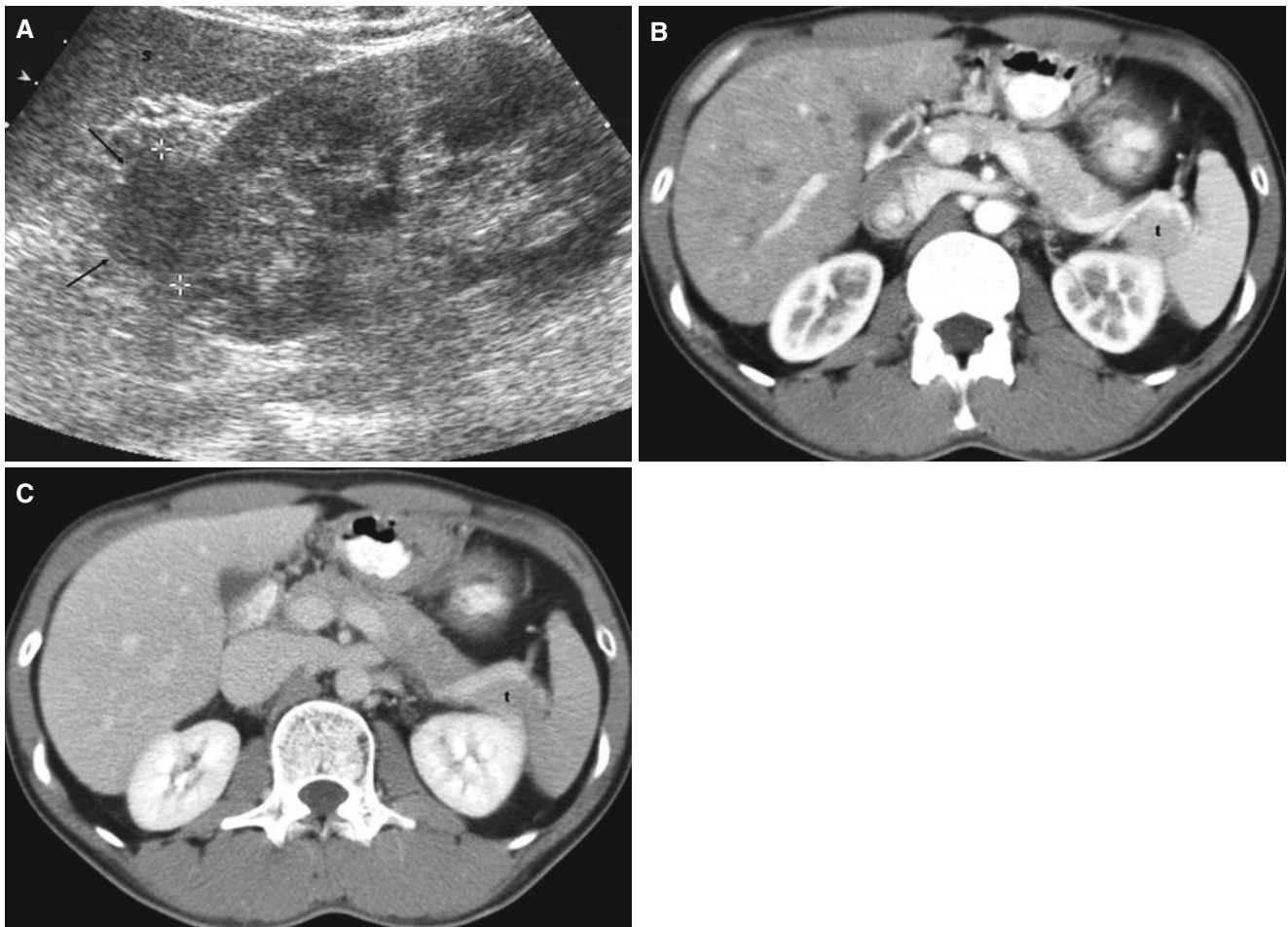
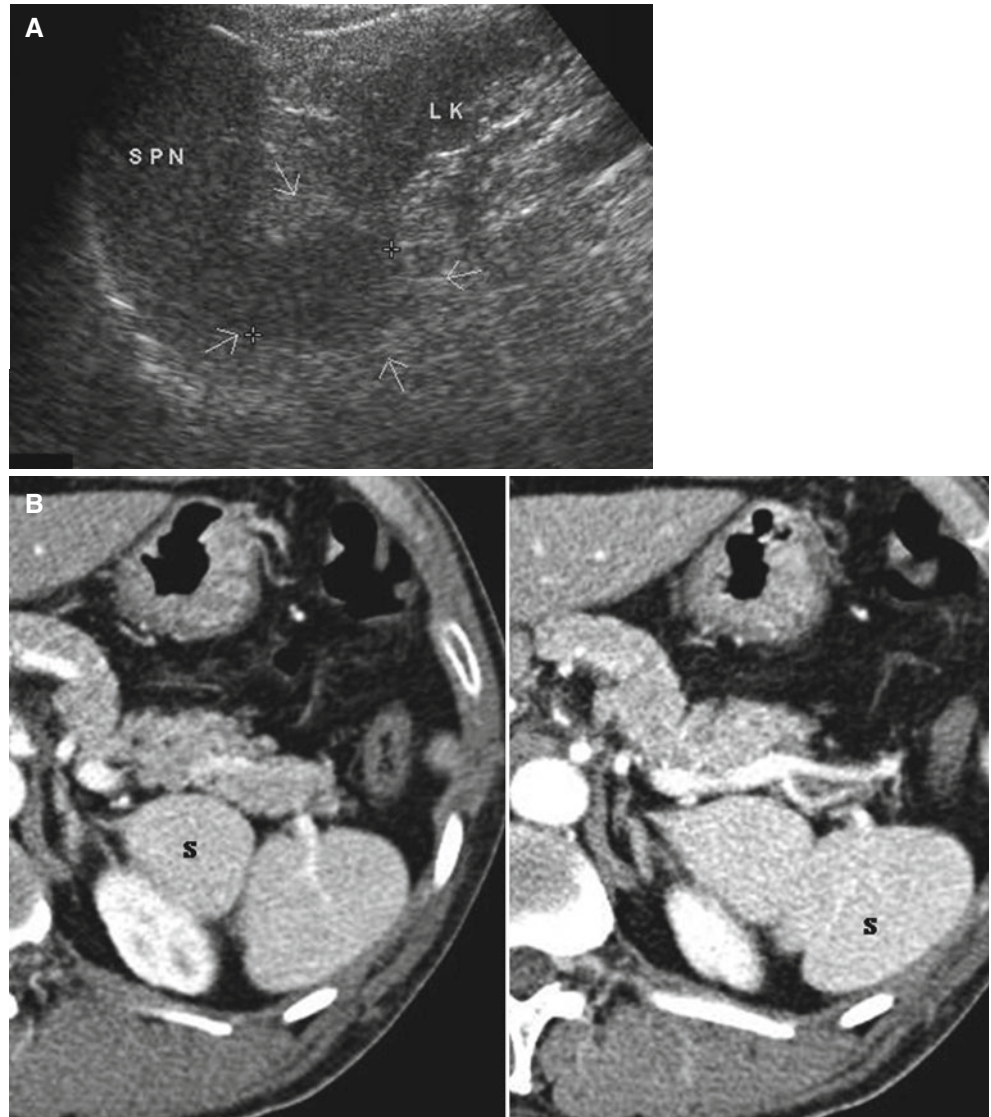


**Fig. 9.6** Renal pseudotumor due to pancreatic tail in a 40-year-old man. (A) Longitudinal US shows a round, hypoechoic mass lesion (black arrows) abutting upper pole of left kidney. s spleen (B and C)

Dynamic contrast-enhanced CT shows no demonstrable mass in the upper polar area of the left kidney. Instead, prominent pancreatic tail (*t*) is seen between the spleen and the left kidney

**Fig. 9.7** Renal pseudotumor due to normal spleen in a 54-year-old-man.

(A) Longitudinal US shows abnormal, round-shaped hypoechoic soft tissue lesion (*white arrows*) between left kidney (*LK*) and spleen (*SPN*). (B) Contrast-enhanced CT shows no demonstrable mass between the left kidney and the spleen (*S*). Medial and inferior part of normal spleen seems to be a cause of this pseudotumor



## 10. Fetal Lobulation

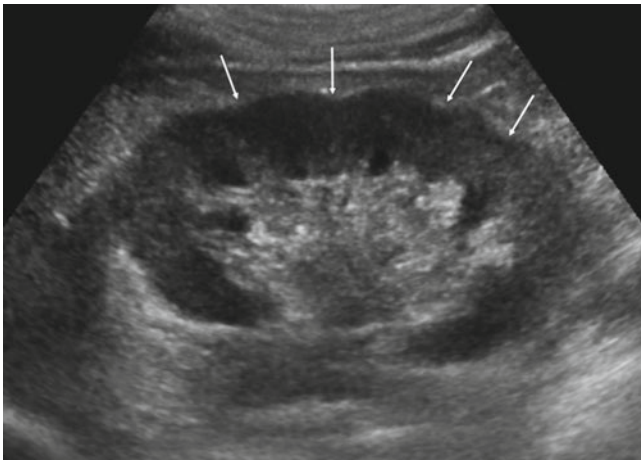


**Fig. 10.1** US image of fetal lobulation in a 75-year-old woman. Longitudinal US of the right kidney shows lobulation with regular indentations (*white arrows*) on the outer margin of the kidney

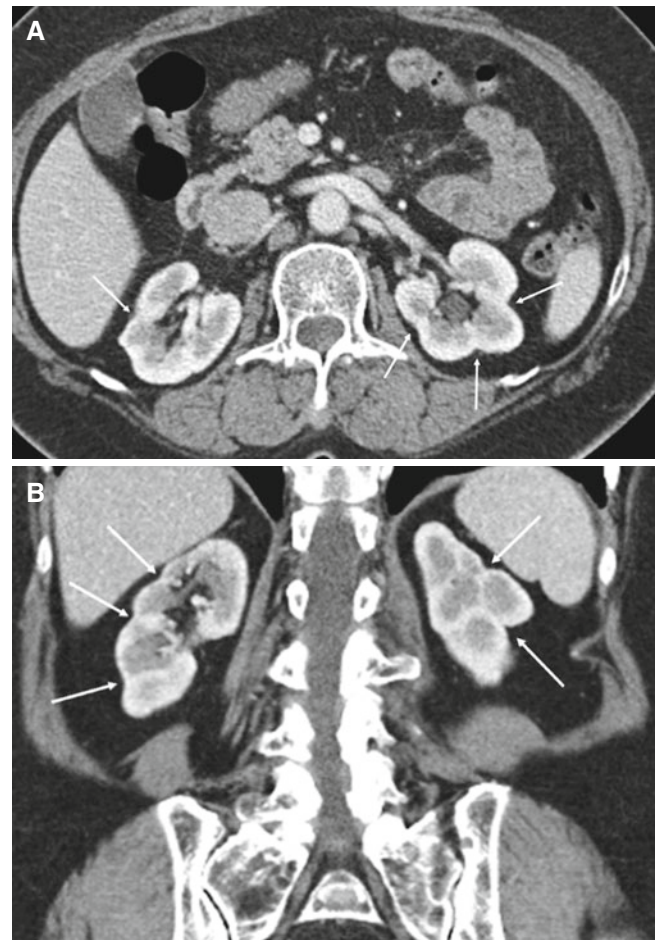


**Fig. 10.2** Contrast-enhanced CT images of fetal lobulation in a 75-year-old woman. (**A** and **B**) Transverse and coronal images show severe lobulated contours and prominent indentations (*white arrows*) in both kidneys

## 11. Hilar Lip



**Fig. 11.1** Suprahilar lip of the right kidney on IVU in a 70-year-old woman. 15-min IVU shows a focal bulging of renal contour in suprahilar portion of the right kidney (*black arrows*). This finding is a normal finding and should not be mistaken for an exophytic renal tumor

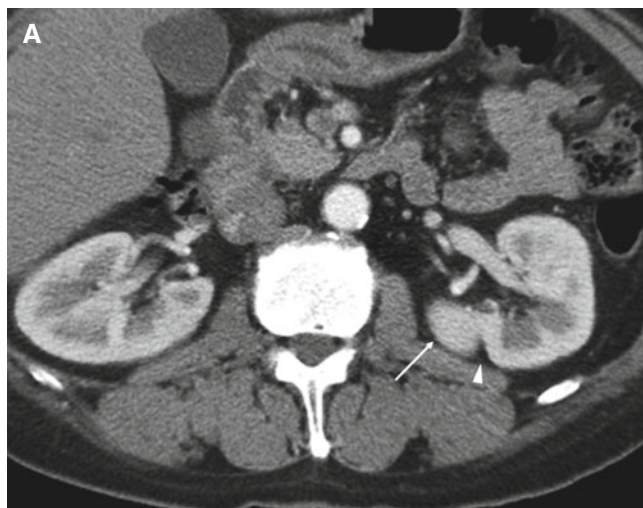


**Fig. 11.2** CT images of hilar lip in a 64-year-old woman. (A and B) Contrast-enhanced CT images in transverse plane show an isolated renal parenchyma (*white arrows*) located at suprahilar portion of the left kidney. This region shows similar contrast enhancement to adjacent normal parenchyma. Note a deep indentation by perirenal fat (*white arrowheads*). (C) On coronal reformatted images, there is a bulging of renal contour (*white arrow*) above the renal hilum

## 12. Junctional Parenchymal Defect

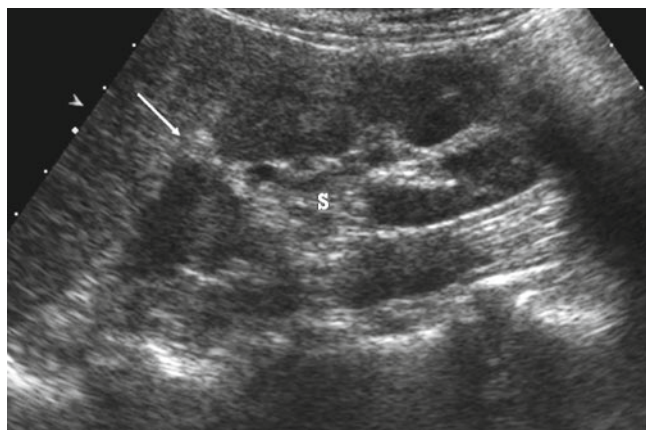


**Fig. 12.1** Junctional parenchymal defect in a 65-year-old man. Longitudinal US of the right kidney in a 65-year-old man shows a wedge-shaped hyperechoic lesion (*white arrow*) in the anteromedial aspect of the upper pole. This lesion is continuous with renal sinus fat (*S*) and shows similar echogenicity

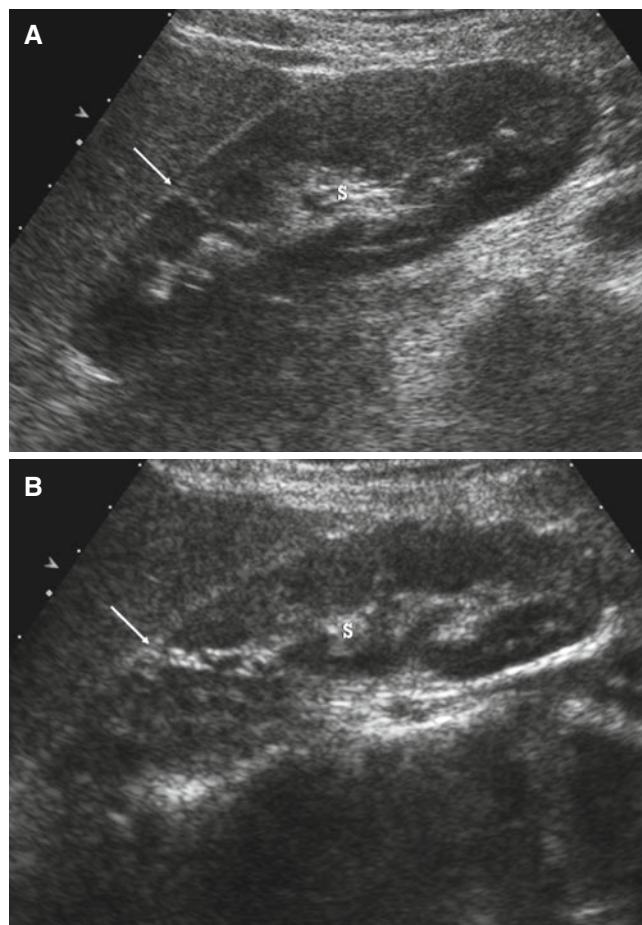


**Fig. 12.2** Junctional parenchymal defect in a 29-year-old woman. (A) Longitudinal US of the right kidney in a 29-year-old woman shows a linear hyperechoic lesion (*white arrow*) with continuity with hyperechoic renal sinus fat (*S*). (B) Longitudinal US medial to A, a triangular-shaped hyperechoic lesion (*white arrow*) is seen, which is continuous with renal sinus fat (*S*)

**Fig. 12.3** US and CT images of a junctional parenchymal defect in a 58-year-old woman. (A) Longitudinal US of the right kidney shows a wedge-shaped, hyperechoic lesion (*white arrow*). This lesion is continuous with renal sinus fat (S). (B) Dynamic contrast-enhanced coronal reformatted CT images reveal a triangular-shaped parenchymal defect (*white arrows*). Renal artery and vein are seen in a junctional parenchymal defect (*black arrowheads*)



### 13. Renal Unidentified Bright Objects on Ultrasonogram

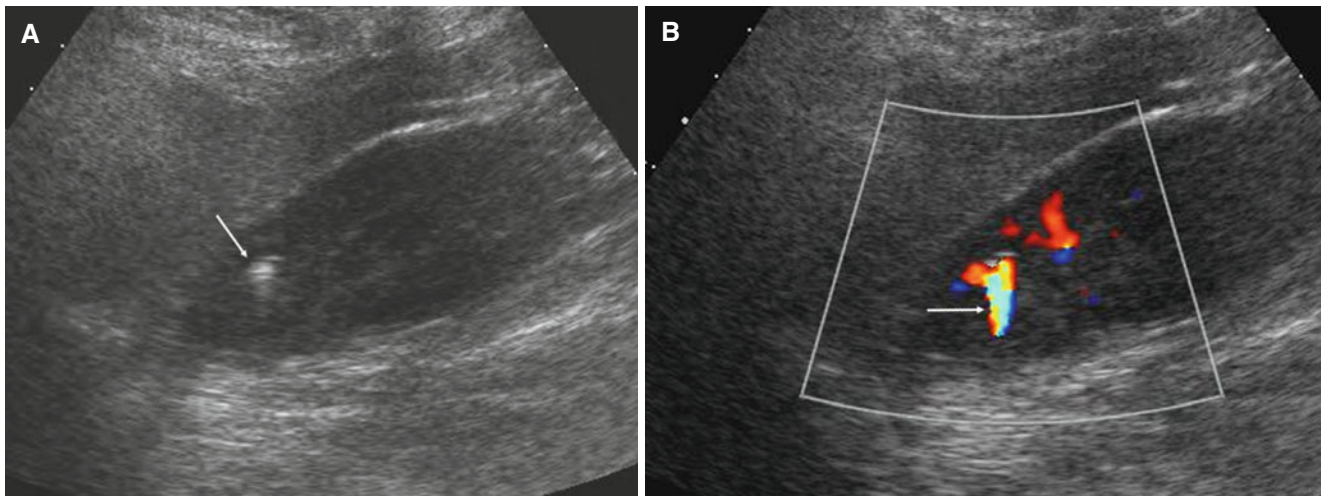


**Fig. 13.1** A UBO with twinkling artifact on US in a 57-year-old woman. (A) Longitudinal US of the right kidney shows an echogenic focus (*white arrow*) in the upper pole, which probably represents twinkling artifact composed of a specular reflective echo from an arcuate

artery. (B) Color Doppler US shows a mixture of colors behind the echogenic focus (*white arrow*). This echogenic focus probably caused by a tiny calcification in the papilla

**Fig. 13.2** An unidentified bright object on US in a 37-year-old woman, probably caused by a small cyst with wall calcification. **(A)** Longitudinal US of the left kidney shows an echogenic focus with suspected echogenic tail (white arrow) in the interpolar area. **(B)** Nonenhanced (left) and contrast-enhanced (right) CT scans reveal a tiny renal cyst (white arrow) with fine calcification (white arrowhead)

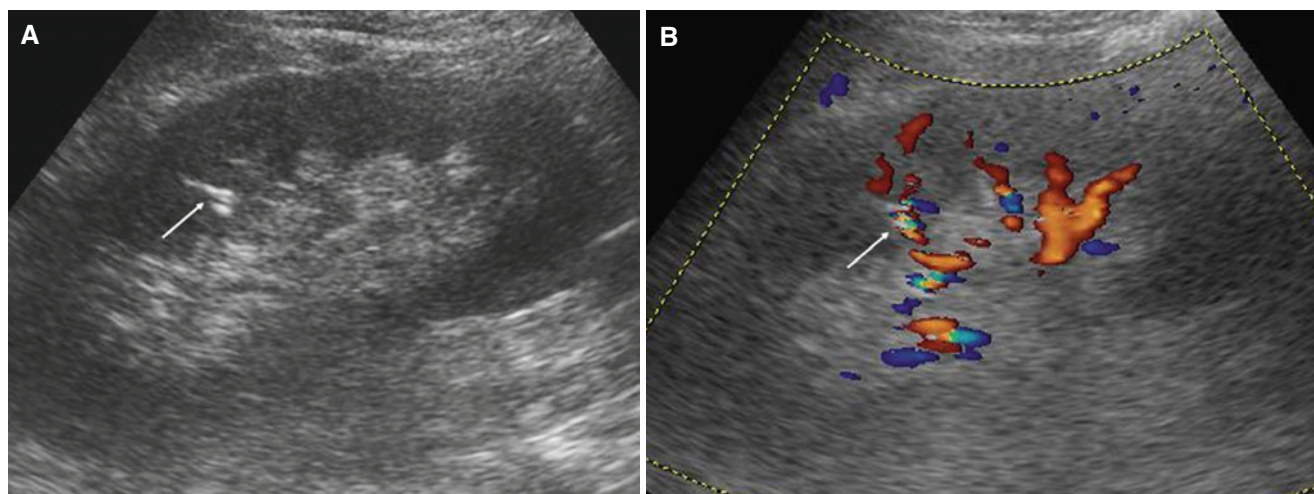
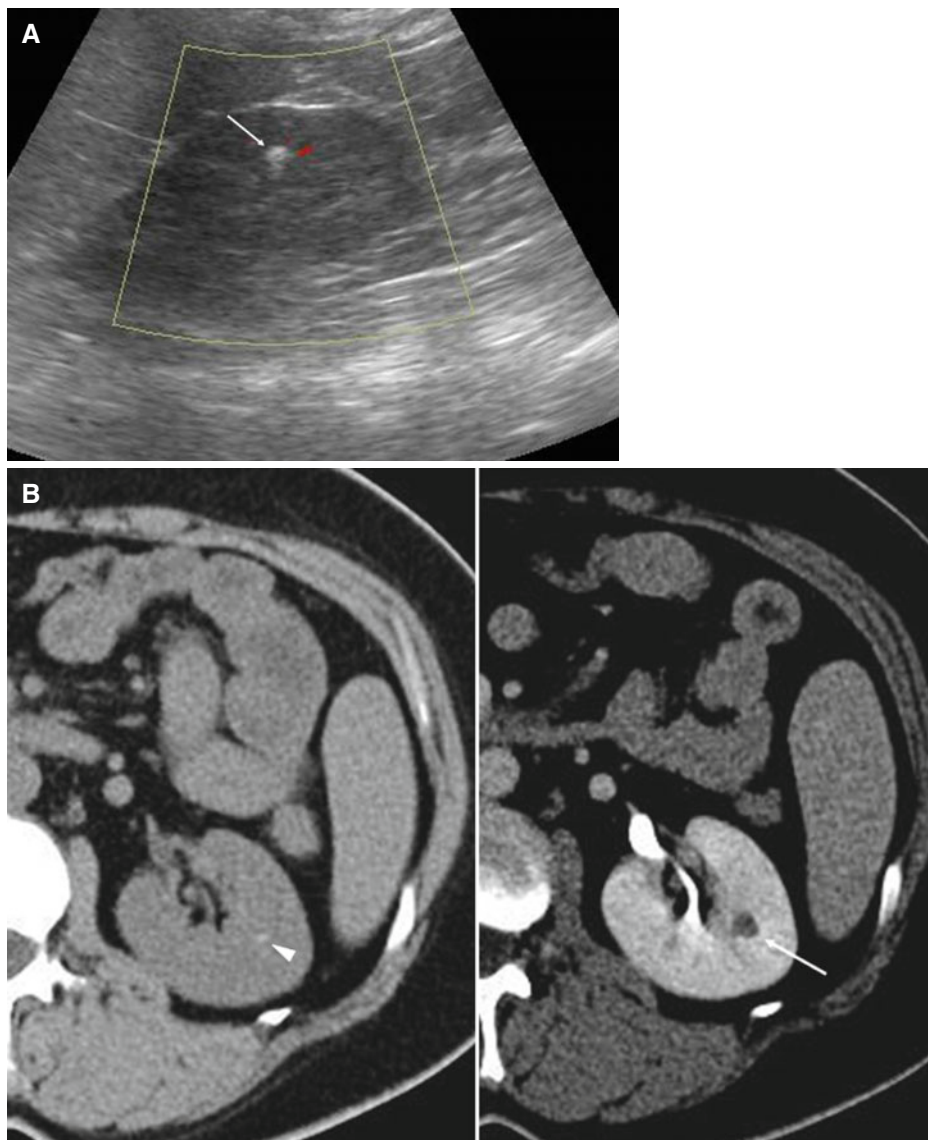


**Fig. 13.3** A UBO on US in a 56-year-old woman, probably caused by a calcification of renal artery associated with DM. **(A)** Longitudinal US of the left kidney shows a linear echogenic focus (white arrow) in the

upper pole. **(B)** Color Doppler US shows a weak twinkling artifact (white arrow) posterior to the echogenic focus

## 14. Sinus Lipomatosis and Prominent Perirenal fat

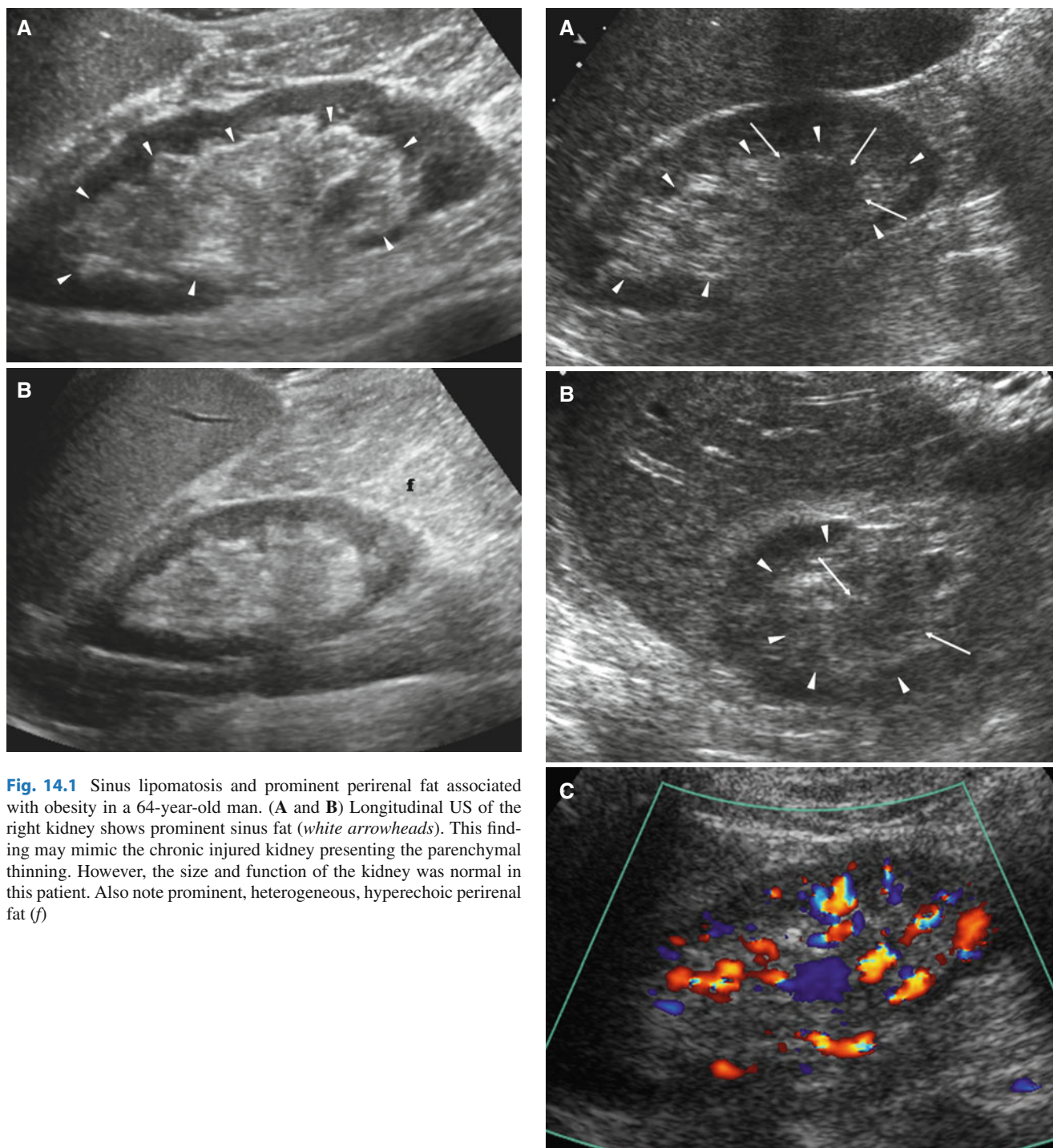


**Fig. 14.1** Sinus lipomatosis and prominent perirenal fat associated with obesity in a 64-year-old man. (**A** and **B**) Longitudinal US of the right kidney shows prominent sinus fat (*white arrowheads*). This finding may mimic the chronic injured kidney presenting the parenchymal thinning. However, the size and function of the kidney was normal in this patient. Also note prominent, heterogeneous, hyperechoic perirenal fat (*f*)

**Fig. 14.2** Prominent and heterogeneous renal sinus fat in a 66-year-old man. (**A** and **B**) Longitudinal and transverse US images of the right kidney show prominent sinus fat (*white arrowheads*) with heterogeneous echogenicity. A region of hypoechoic sinus fat (*white arrows*) may mimic urothelial tumor of the renal pelvis. (**C**) Color Doppler US shows normal interlobar vessels passing through the hypoechoic renal sinus fat without stretching or displacement

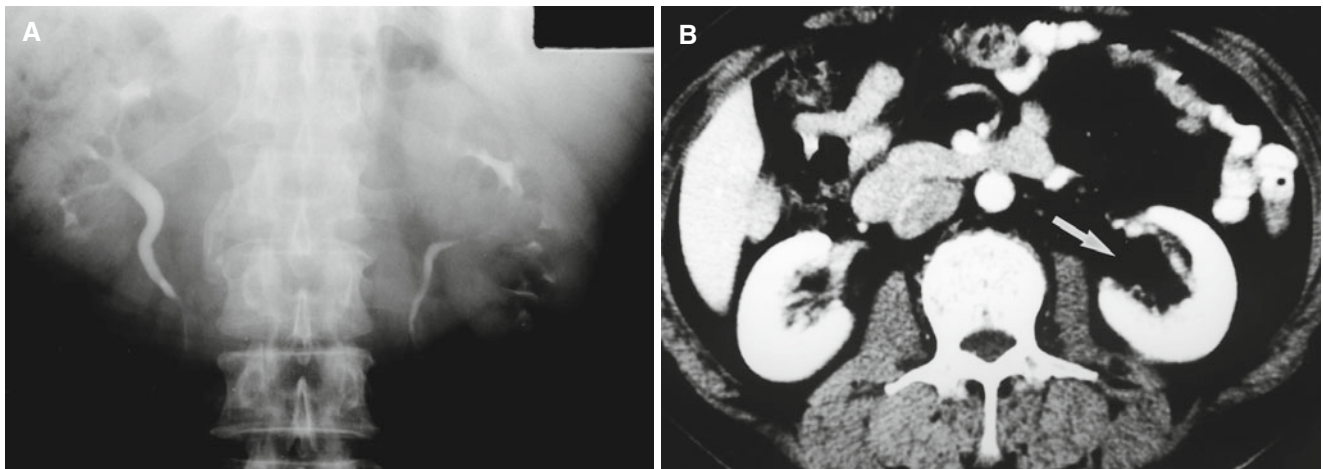


**Fig. 14.3** Prominent renal sinus fat in a 57-year-old man with liver cirrhosis. (A) IVU shows lower position of the left kidney due to splenomegaly and indistinct calyceal infundibula in the left kidney.

(B) Contrast-enhanced CT reveals prominent sinus fat in the left kidney (*white arrow*), which is the cause of compression effect on calyceal infundibula

## 15. Pseudohydronephrosis

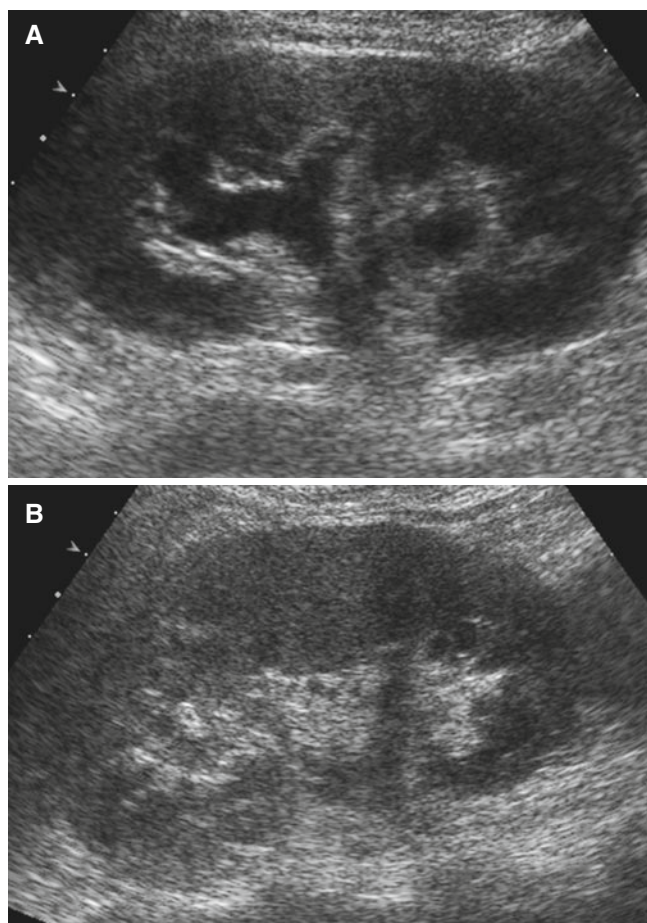


**Fig. 15.1** Transient hydronephrosis in a 44-year-old woman who had a full bladder for pelvic US. (A) US of the left kidney shows dilatation of the pelvocalyces when the urinary bladder was full. (B) Repeated US after voiding shows disappeared pelvocaliceal dilatation



**Fig. 15.2** US finding of pseudohydronephrosis by multiple parapelvic cysts (white arrows) in a 75-year-old woman. Parapelvic cysts may be differentiated from hydronephrosis by absence of communication among the cystic lesions

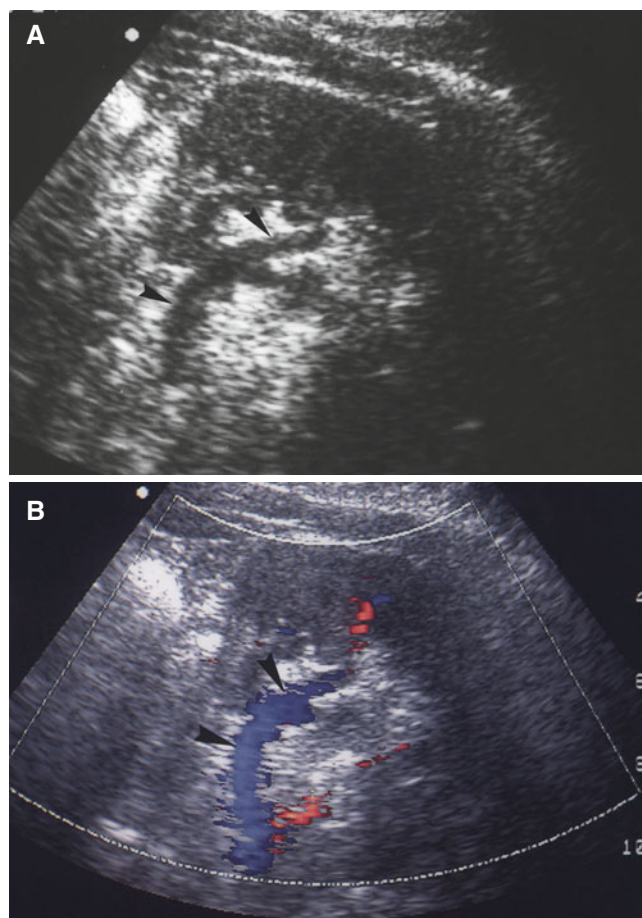


**Fig. 15.3** US findings of pseudohydronephrosis by prominent renal vessels in a 27-year-old man. (A) US of the left kidney in transverse plane shows a tubular anechoic structure (black arrowheads) in the renal hilar region mimicking dilated pelvocaliceal system. (B) Color Doppler US reveals flow signal in the tubular structure (black arrowheads) confirming that the structure is a blood vessel and is not dilated pelvocalyces

## 16. Ureter: Normal Findings and Variations



**Fig. 16.1** Medial deviation of the ureters due to large psoas muscle in a 53-year-old man. IVU shows medial deviation of bilateral distal ureters probably due to prominent psoas muscles



**Fig. 16.2** Medial deviation of the ureter in a 33-year-old man. IVU shows medial deviation of the right proximal ureter (*black arrows*) without any abnormality

## 17. Urinary Bladder: Normal Findings and Variations

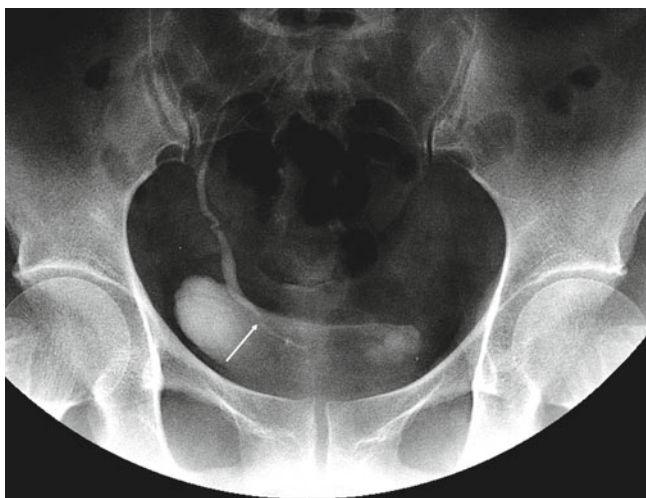


**Fig. 17.1** Ureteral jet on IVU in a 52-year-old woman. IVU shows a jet of urine from the ureteral orifice (*white arrow*) into the bladder



**Fig. 17.3** Ureteral jet on CT in a 27-year-old man. Contrast-enhanced CT shows jetting of opacified urine (*black arrow*) from the left ureteral orifice into the bladder

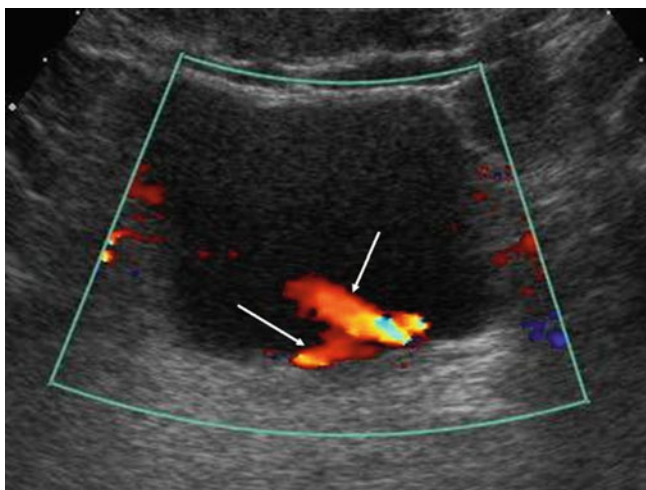


**Fig. 17.2** Ureteral jet on color Doppler US in a 56-year-old man. Color Doppler US of the bladder shows jetting of urine (*white arrows*) from the both ureteral orifices. This finding of ureteral jet virtually exclude the possibility of significant obstruction of the urinary tract

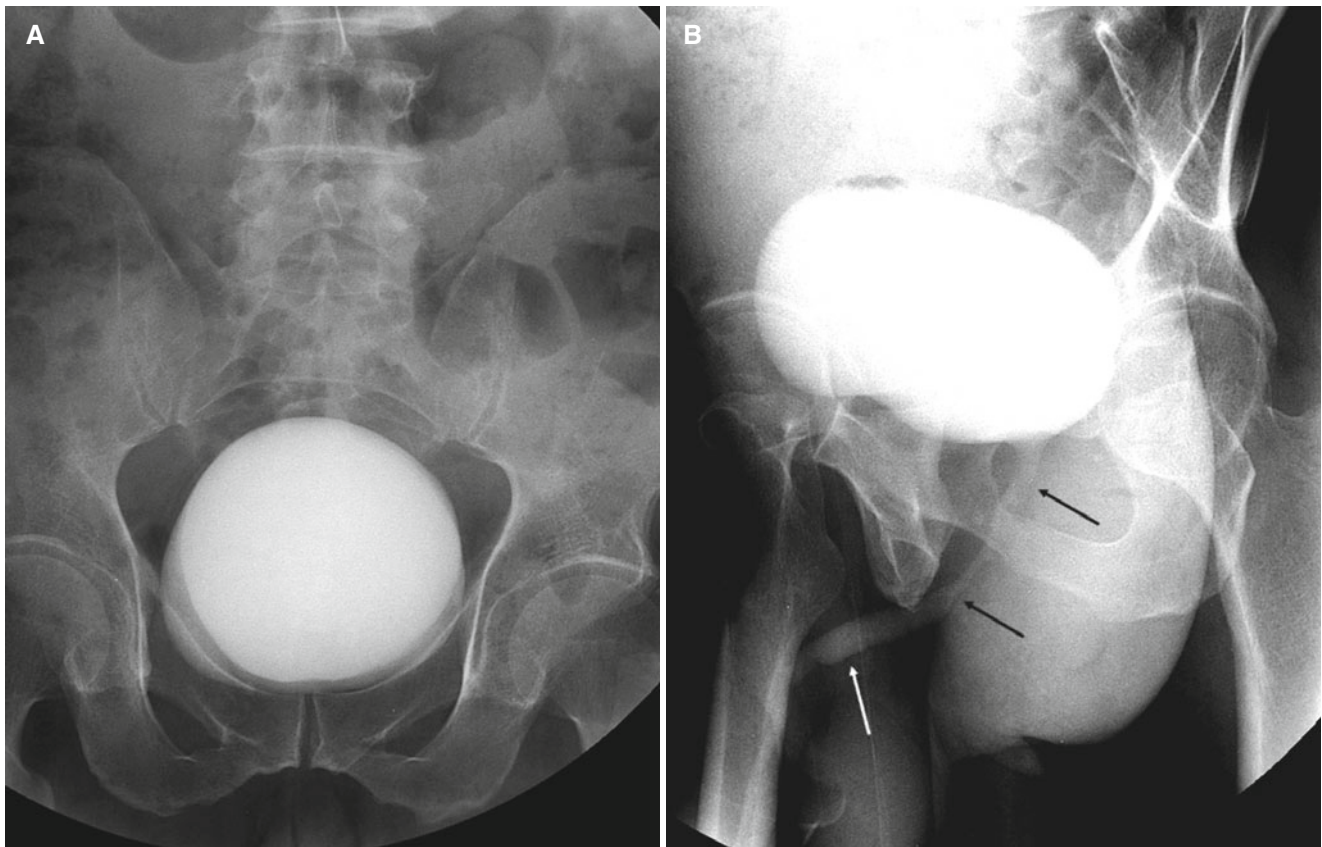


**Fig. 17.4** Normal bladder on VCU in a 49-year-old man. VCU images in resting (**A**) and voiding (**B**) states show smooth contour of the bladder and absence of vesicoureteral reflux. Also note normal urethra on *B* (arrows)

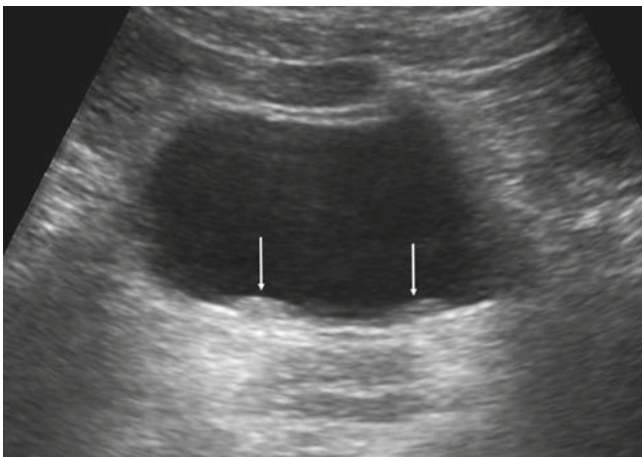


**Fig. 17.5** Normal bladder on US in a 57-year-old woman. US of the bladder in transverse plane shows prominent bladder mucosa at the ureterovesical junctions on both sides (white arrows)

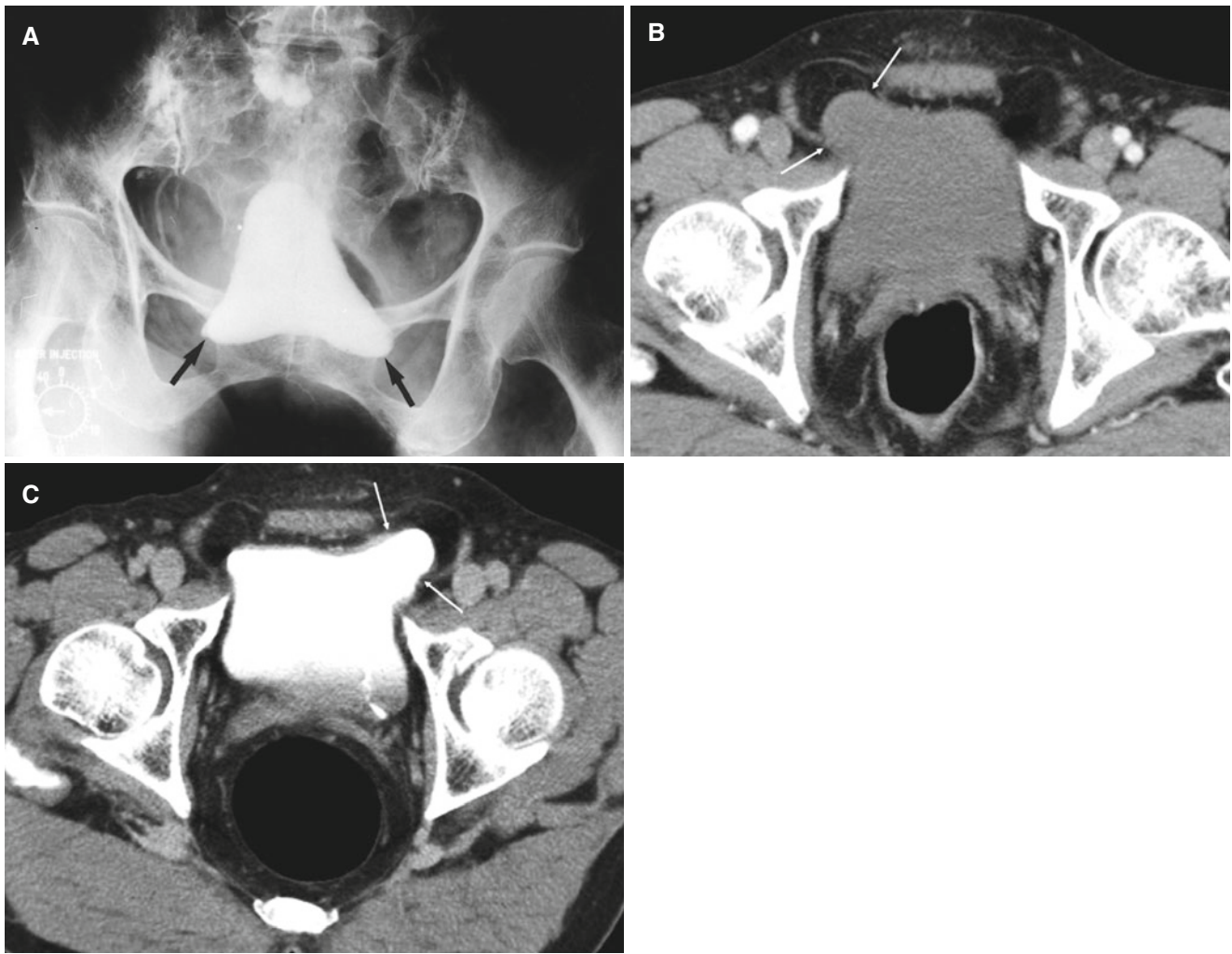


**Fig. 17.6** Bladder ears. (A) A 75-year-old woman who underwent radical hysterectomy and radiation therapy for uterine cervical carcinoma. IVU shows protrusion of the bladder into both inguinal rings (black arrows). (B and C) Bilateral bladder ear in a 63-year-old man.

Dynamic contrast-enhanced CT demonstrates protrusion of the both inferolateral aspects of the bladder into the inguinal rings (white arrows)

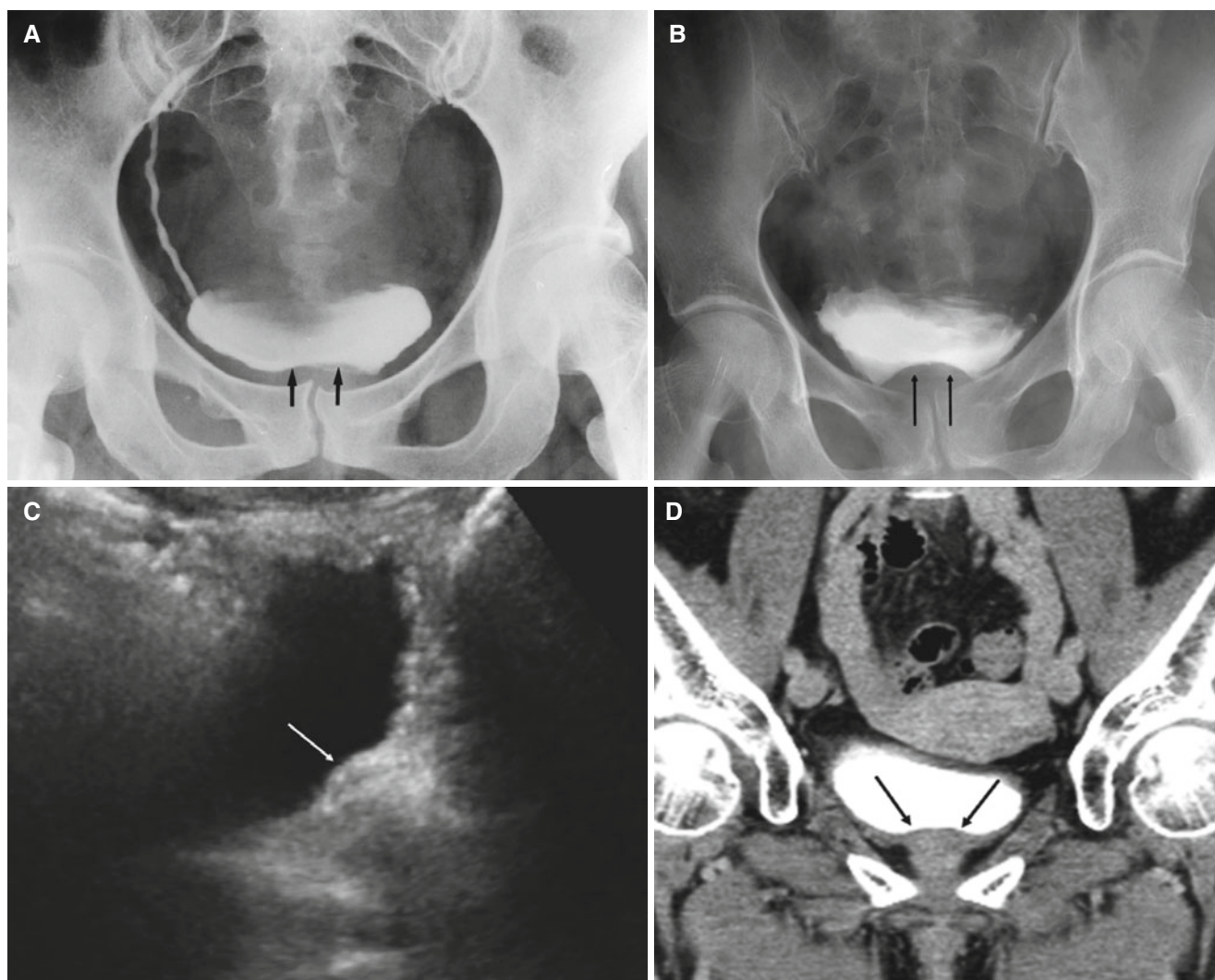


**Fig. 17.7** Female prostate. IVUs in 41- (A) and 81- (B) year-old women show smooth elevations of the bladder necks (*black arrows*). This IVU finding is called *female prostate* because it closely mimics a finding of prostatic enlargement in the man. (C) Longitudinal US of the bladder in

a 31-year-old woman shows elevation of the bladder neck (*white arrow*) due to prominent soft tissue of the proximal urethra. (D) Contrast-enhanced coronal reformatted CT images reveal elevation of the bladder neck (*black arrows*) due to prominent soft tissue of the proximal urethra

Radiology Illustrated: Uroradiology

Kim, S.H. (Ed.)

2012, XIV, 1335 p. 1433 illus., 326 illus. in color.,

Hardcover

ISBN: 978-3-642-05321-4